JCI insight

RESEARCH ARTICLE

Ganglionic GFAP+ glial Gq-GPCR signaling enhances heart functions in vivo

Alison Xiaoqiao Xie, Jakovin J. Lee, and Ken D. McCarthy

Department of Pharmacology, School of Medicine, University of North Carolina at Chapel Hill, Chapel Hill, North Carolina, USA.

The sympathetic nervous system (SNS) accelerates heart rate, increases cardiac contractility, and constricts resistance vessels. The activity of SNS efferent nerves is generated by a complex neural network containing neurons and glia. Gq G protein–coupled receptor (Gq-GPCR) signaling in glial fibrillary acidic protein–expressing (GFAP+) glia in the central nervous system supports neuronal function and regulates neuronal activity. It is unclear how Gq-GPCR signaling in GFAP+ glia affects the activity of sympathetic neurons or contributes to SNS-regulated cardiovascular functions. In this study, we investigated whether Gq-GPCR activation in GFAP+ glia modulates the regulatory effect of the SNS on the heart; transgenic mice expressing Gq-coupled DREADD (designer receptors exclusively activated by designer drugs) (hM3Dq) selectively in GFAP+ glia were used to address this question in vivo. We found that acute Gq-GPCR activation in peripheral GFAP+ glia significantly accelerated heart rate and increased left ventricle contraction. Pharmacological experiments suggest that the glial-induced cardiac changes were due to Gq-GPCR activation in satellite glial cells within the sympathetic ganglion; this activation led to increased norepinephrine (NE) release and beta-1 adrenergic receptor activation within the heart. Chronic glial Gq-GPCR activation led to hypotension in female *Gfap*-hM3Dq mice. This study provides direct evidence that Gq-GPCR activation in peripheral GFAP+ glia regulates cardiovascular functions in vivo.

Introduction

To a large degree, the sympathetic nervous system (SNS) stabilizes blood pressure and mediates the cardiovascular adjustments required of various behaviors or stresses (1, 2). Sympathetic nerve activity (SNA) is elevated in old age (3) and in cardiovascular-related diseases (4) including hypertension (5, 6), arrhythmias (7, 8), obesity, obstructive sleep apnea, and congestive heart failure (9, 10). An understanding of the diverse cellular and molecular components of SNS control of cardiovascular functions is needed to enhance the search for new targets of cardiovascular disease (CVD) drug therapies.

The SNS consists of preganglionic neurons located in the spinal cord and postganglionic neurons or their neuro-endocrine equivalent (adrenal glands). Although SNA is mainly considered a product of integration by neuronal networks, recent evidence suggests that Gq G protein–coupled receptor (Gq-GPCR) activation in glial fibrillary acidic protein–expressing (GFAP+) glia (CNS astrocytes and non-myelinating peripheral glia) also contributes to homeostatic control of blood gases (11–13) and gastrointestinal motility (14, 15) via modulation of local neuronal activity. Recently, we showed that selective activation of Gq-GPCR signaling in GFAP+ glia in vivo led to acute changes in autonomic functions, including increases in heart rate and blood pressure (16). Here, we test the hypothesis that Gq-GPCR activation in SNS GFAP+ glia enhances SNS-driven cardiac functions in vivo.

To test this hypothesis, we used a transgenic mouse expressing the Gq-coupled DREADD (designer receptor exclusively activated by designer drugs) under control of a GFAP minimal promoter (*Gfap*-hM3Dq mice; ref. 16). The hM3Dq receptor exhibits no constitutive activity and can only be activated by the otherwise bio-inert small molecule clozapine-N-oxide (CNO) (17), providing a unique model for assessing the role of Gq-GPCR activation in GFAP+ cells. Acute CNO administration (0.5 mg/kg) resulted in robust increases in beta-1 adrenergic receptor–mediated heart rate and left ventricular contractility, suggesting activation of the SNS. Pharmacological experiments revealed that these CNO-induced cardiac changes were due to Gq-GPCR activation in GFAP+ satellite glial cells (SGCs) in the sympathetic ganglia. Moreover, chronic CNO administration in *Gfap*-hM3Dq mice led to hypotension. Our data reveal a function of peripheral GFAP+ glial Gq-GPCR activation in short-term and

Conflict of interest: The authors have declared that no conflict of interest exists.

Submitted: September 8, 2016
Accepted: December 13, 2016
Published: January 26, 2017

Reference information:
JCI Insight. 2017;2(2):e90565.
doi:10.1172/jci.insight.90565.

long-term cardiovascular regulation. These findings are also the first demonstration to our knowledge of the function of SGCs in sympathetic ganglia.

Results

CNO activates Gq-GPCR signaling pathways in SNS GFAP$^+$ glia of Gfap-hM3Dq mice. *Gfap*-hM3Dq mice (16) (Figure 1A) were used to activate the Gq-GPCR signaling pathway in GFAP$^+$ glia in vivo (Figure 1B). Previous studies indicate that hM3Dq expression in *Gfap*-hM3Dq mice is restricted to GFAP$^+$ glia in both the CNS and peripheral nervous system (PNS), including astrocytes in the CNS and ganglionic glia in the PNS (16). To confirm the functionality of this receptor, we examined whether CNO could induce intracellular Ca^{2+} elevation (an event downstream of Gq-GPCR activation; ref. 18) in GFAP$^+$ glia in the SNS. First, we examined whether CNO induced intracellular Ca^{2+} elevations in astrocytes in the rostral ventrolateral medulla (RVLM), a brain region that contributes greatly to SNA (19, 20) (Figure 1, C–E). Sulforhodamine 101 (SR-101) is a common astrocyte marker both in situ (16, 21) and in vivo (22) and selectively labels medulla astrocytes in acute brainstem slices in *Glt1*-eGFP mice (Supplemental Figure 1; supplemental material available online with this article; https://doi.org/10.1172/jci.insight.90565DS1); SR-101 was used in this experiment to label medulla astrocytes from *Gfap*-hM3Dq mice (Figure 1C). OGB-1 was loaded into medulla astrocytes to monitor their cytoplasmic Ca^{2+} activity (Figure 1C). Three doses of CNO (5, 10, and 20 μM) were bath-applied to brainstems slices; a single brain slice only received one of the CNO doses. Astrocytes that responded with $[Ca^{2+}]_i$ elevations to CNO (Figure 1D, asterisks) were counted. At the end of each experiment, a cocktail of Gq-GPCR agonists (DHPG, ATP, carbachol, histamine; 10 μM each; Figure 1D) was used to reveal the viability of astrocytes in acute slices. The majority of the SR-101 and OGB-1 double-positive astrocytes responded to the agonist cocktail in brainstem slices from *Gfap*-hM3Dq mice (Figure 1D) and littermate control mice; astrocytes that did not respond to agonist cocktail were excluded from further analysis. A maximally effective concentration of CNO increased Ca^{2+} in approximately 50% of viable astrocytes (Figure 1E), demonstrating hM3Dq expression in brainstem GFAP$^+$ glia. No CNO-evoked Ca^{2+} elevations were observed in brainstem slices from littermate controls (Figure 1E).

We next examined whether HA-hM3Dq–expressing SGCs in sympathetic ganglia exhibited CNO-induced intracellular Ca^{2+} elevations using superior cervical ganglion explants as a model (Figure 1, F and G). *Gfap*-GcaMP3 transgenic mice were developed to monitor Ca^{2+} dynamics in ganglionic SGCs (Supplemental Figure 2A). Superior cervical ganglia were isolated from *Gfap-GcaMP3$^{+/-}$::Gfap-hM3Dq$^{+/-}$* mice and cultured as explants for up to 7 days; experiments were performed between days 5 and 7 (Supplemental Figure 2). Immunohistochemistry data showed that GcaMP3 was expressed in brain lipid binding protein–positive (BLBP$^+$) SGCs (23) but not in postganglionic neuronal soma or tyrosine hydroxylase–positive (TH$^+$) neuronal processes (Supplemental Figure 2, B and C). CNO (10 μM) induced Ca^{2+} elevations in GcaMP3$^+$ SGCs in ganglionic explants isolated from *Gfap-GcaMP3$^{+/-}$::Gfap-hM3Dq$^{+/-}$* mice (Figure 1G and Supplemental Figure 2, D and E). No CNO-evoked Ca^{2+} elevations were observed in GcaMP3$^+$ control ganglia explants isolated from littermate *Gfap-GcaMP3$^{+/-}$::Gfap-hM3Dq$^{-/-}$* mice (Figure 1G and Supplemental Figure 2E). Na-ATP (10 μM) was used to verify the responsiveness of SGCs and induced similar Ca^{2+} responses from the majority of SGCs in ganglia explants from both *Gfap*-hM3Dq mice and littermate controls (Figure 1G and Figure 2F). Interestingly, none of the SGCs responded to a cocktail of common Gq-GPCR agonists including DHPG, histamine, and carbachol (10 μM each) (Supplemental Figure 2D), suggesting the lack of endogenous GPCRs for these ligands in the SGCs in cultured superior cervical ganglia.

Acute CNO administration in vivo in Gfap-hM3Dq mice leads to beta-1 adrenergic receptor–sensitive, SNS-driven cardiac activation. We next tested whether the CNO-induced tachycardia (16) was due to the activation of SNS (Figure 2A). SNS regulates heart rate via activation of beta adrenergic receptors (24), which can be directly blocked by (S)-atenolol (25). Therefore, we administered 10 mg/kg (S)-atenolol i.p. to *Gfap*-hM3Dq mice, a dose that reliably blocks isoprenaline (a beta-1 adrenergic receptor agonist) induced tachycardia (25) (Figure 2B, 5 μg/kg BW, 6 tests in 3 mice). CNO injection in *Gfap*-hM3Dq mice induced significant increases in heart rate compared with their littermate controls (16) (Figure 2C). Pre-administration of (S)-atenolol 10 minutes prior to CNO (i.p. 0.5 mg/kg) abolished CNO-induced tachycardia in *Gfap*-hM3Dq mice, suggesting that CNO-induced tachycardia is due to downstream activation of beta-1 receptors (Figure 2C). No CNO-induced changes in heart rate were observed in littermate control mice (Figure 2C).

SNS activation enhances left ventricle contraction (26). We examined whether glial Gq-GPCR activation leads to changes in left ventricular contractility in conscious *Gfap*-hM3Dq mice using echocardiography. *Gfap*-hM3Dq mice and their littermate controls received CNO injections (0.5 mg/kg, i.p.) 15 minutes

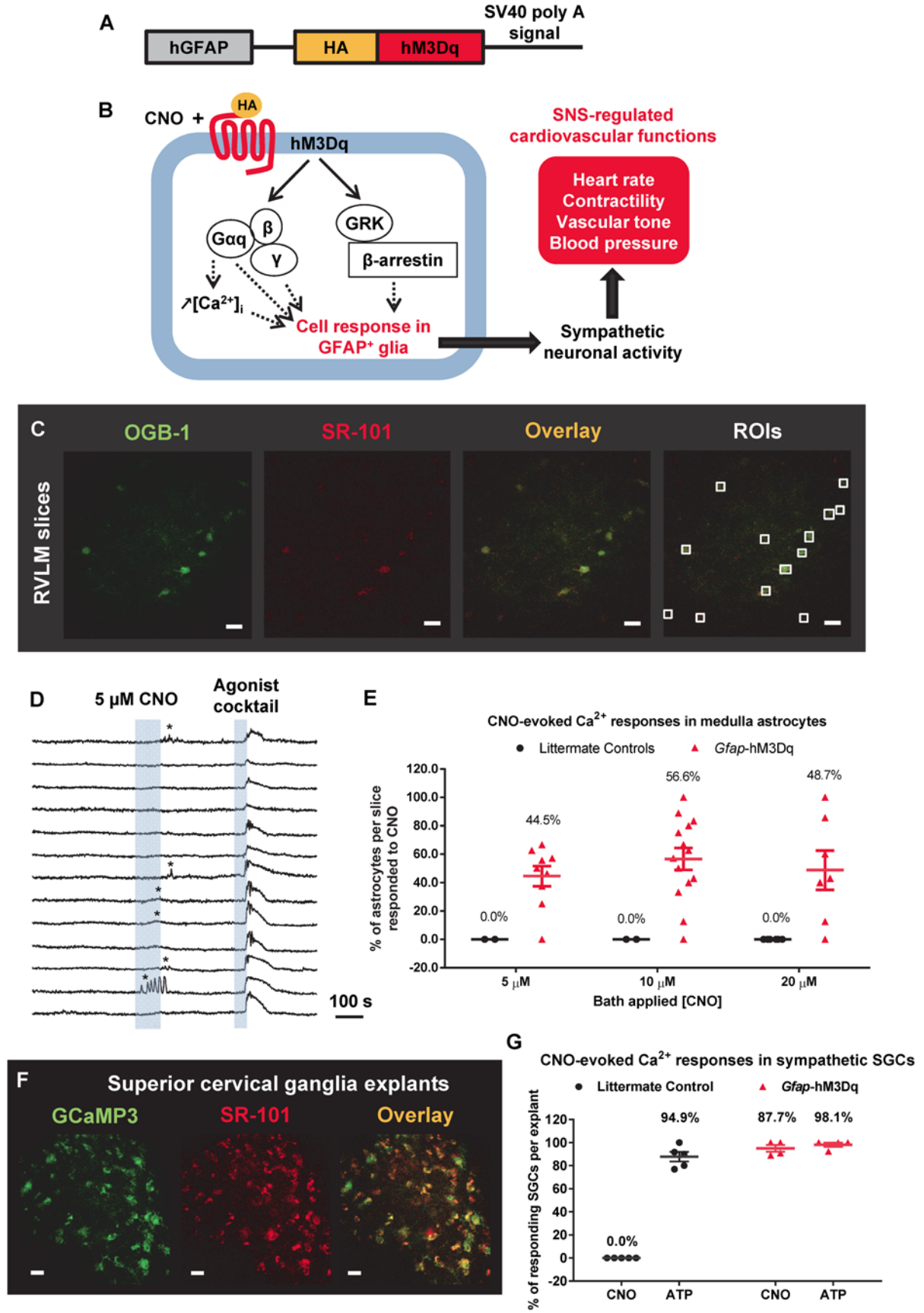

Figure 1. Selective and functional expression of hM3Dq by GFAP⁺ glia in *Gfap*-hM3Dq mice. (**A**) Schematic of transgene containing hemagglutinin-tagged (HA-tagged) hM3Dq driven by the fragment of human glial fibrillary acidic protein promoter (hGFAP). (**B**) Schematic of the hypothesis that pharmacogenetic activation of Gq-GPCR signaling pathways in GFAP⁺ glia leads to changes in sympathetic neuronal activity and changes in cardiovascular functions

in vivo. GRK, GPCR kinase. (**C**) OGB-1 loading in SR-101–labeled medulla astrocytes in acute medulla slices (original magnification, 60×; scale bars: 20 μm). RVLM, rostral ventrolateral medulla. (**D**) Representative data of bath-applied CNO–induced intracellular Ca^{2+} elevations in a subset of medulla astrocytes in acute brainstem slices from *Gfap*-hM3Dq mice (9 experiments conducted). (**E**) Percentage of medulla astrocytes that responded to CNO with intracellular Ca^{2+} elevations in *Gfap*-hM3Dq mice and littermate control mice. (**F**) Confocal image showing GCaMP3 signal from SR-101–labeled $GFAP^+$ SGCs in superior cervical ganglia explant culture isolated from *Gfap-GCaMP3*$^{+/-}$*::Gfap-hM3Dq*$^{+/-}$ mice (original magnification, 60×; scale bars: 20 μm). (**G**) Quantification of percentage of superior cervical ganglionic SGCs that exhibited intracellular Ca^{2+} elevations in response to CNO and ATP (10 μM each) from both *Gfap-GCaMP3*$^{+/-}$*::Gfap-hM3Dq*$^{+/-}$ mice and *Gfap-GCaMP3*$^{+/-}$ littermate control mice (*Gfap-GCaMP3*$^{+/-}$*::Gfap-hM3Dq*$^{+/-}$: 48 cells/4 explants/2 mice; *Gfap-GCaMP3*$^{+/-}$ littermate controls: 57 cells/5 explants/2 mice).

prior to echocardiogram recordings (Figure 2D). Glial Gq-GPCR activation significantly increased ejection fraction (EF) and fraction shortening (FS) in *Gfap*-hM3Dq mice, but not in littermate control mice (Figure 2, E and F); no differences in the baseline echocardiogram measurements were observed between *Gfap*-hM3Dq mice and littermate control mice (Figure 2, E and F). CNO-induced changes in EF and FS were also abolished by pretreatment with (S)-atenolol (10 mg/kg) 10 minutes prior to CNO (Figure 2, E and F). Based on these data, we concluded that glial Gq-GPCR activation induced increases cardiac rate and contractility requires SNS activation (Figure 2G).

CNO-induced tachycardia is due to NE released by cardiac sympathetic nerves as opposed to the adrenal medulla. We next asked whether the CNO-induced tachycardia required sympathetic innervation into the heart. To remove the sympathetic innervation of the heart, we injected *Gfap*-hM3Dq mice and littermate controls with 6-hydroxydopamine (6-OHDA) to induce peripheral sympathectomy (27) (Figure 3A). When injected in periphery, 6-OHDA enters noradrenergic terminals via NE reuptake transporters and destroys sympathetic terminals (28). This treatment spares cholinergic neurons, Schwann cells, non-myelinating glia including ganglionic SGCs, endothelial cells, and adrenal medulla (28, 29). In both 6-OHDA–injected *Gfap*-hM3Dq and their littermate controls, tyramine-induced tachycardia was significantly suppressed as compared with those in vehicle-injected controls, indicating successful sympathectomy (29) (Figure 3B). CNO-induced tachycardia was largely abolished in 6-OHDA–injected *Gfap*-hM3Dq mice (Figure 3C), suggesting that the increases in heart rate following glial Gq-GPCR activation are dependent on sympathetic innervation into the heart. CNO-induced tachycardia in *Gfap*-hM3Dq mice was unaffected following bilateral adrenalectomy (ADX) (Figure 3D). These findings suggest that glial activation–induced tachycardia results from NE release from sympathetic nerve terminal, as opposed to catecholamine release from adrenal glands (Figure 3E); these data are consistent with the lack of HA-hM3Dq expression in adrenal glands in *Gfap*-hM3Dq mice (16).

CNO-induced cardiac changes in Gfap-hM3Dq mice are due to the activation of peripheral $GFAP^+$ glia. CNO is a small molecule that readily crosses the blood-brain barrier (BBB) (17). Peripheral injections of CNO activate $GFAP^+$ glia in the CNS and the PNS, both of which have the potential to modulate SNS-driven cardiovascular functions. Since CNO-induced activation of hM3Dq can be blocked by muscarinic acetylcholine receptor (mAChR) antagonists (17), we used trospium chloride, a peripherally restricted mAChR antagonist (30), to determine whether the cardiovascular effects of CNO were mediated centrally or peripherally. Experiments were performed to verify that at the dose used, trospium chloride does not inhibit CNO-induced hM3Dq activation in CNS astrocytes. Using 2-photon imaging in vivo (31), we compared astrocytic CNO-induced Ca^{2+} elevations in the presence and absence of pretreatment with trospium chloride (Figure 4A). We did not find any significant differences in amplitude or frequency of CNO-induced Ca^{2+} oscillations between cortical astrocytes with and those without trospium chloride (Figure 4B, 0.04 Hz vs. 0.043 Hz). These findings indicate that at the dose used, trospium chloride does not block CNO-induced Gq-GPCR activation in CNS astrocytes.

Pretreatment of trospium chloride abolished CNO-induced tachycardia in *Gfap*-hM3Dq mice (Figure 4C). Thus, Gq-GPCR activation in peripheral $GFAP^+$ glia, not CNS astrocytes, appears to be responsible for CNO-induced tachycardia in *Gfap*-hM3Dq mice. Furthermore, blockade of ganglionic transmission with a cocktail of hexamethonium (HEX) and chlorisondamine (CHL) (32) (20 mM and 5 mM, respectively) did not block the CNO-induced cardiovascular phenotype (Figure 4E). However, this cocktail of blockers did block the prazosin-induced baroreceptor reflex (Figure 4D), demonstrating that the cocktail effectively blocked ganglionic transmission. Collectively, these findings strongly support the hypothesis that the activation of peripheral $GFAP^+$ glia mediates CNO-induced increases in heart rate in *Gfap*-hM3Dq mice (Figure 4G).

hM3Dq-mediated Gq-GPCR activation in medulla astrocytes does not contribute to CNO-induced tachycardia in vivo. Approaches to selectively activate hM3Dq-mediated Gq-GPCR signaling pathways in CNS astrocytes were devised (Supplemental Figure 3). Three experimental strategies were used to selectively activate

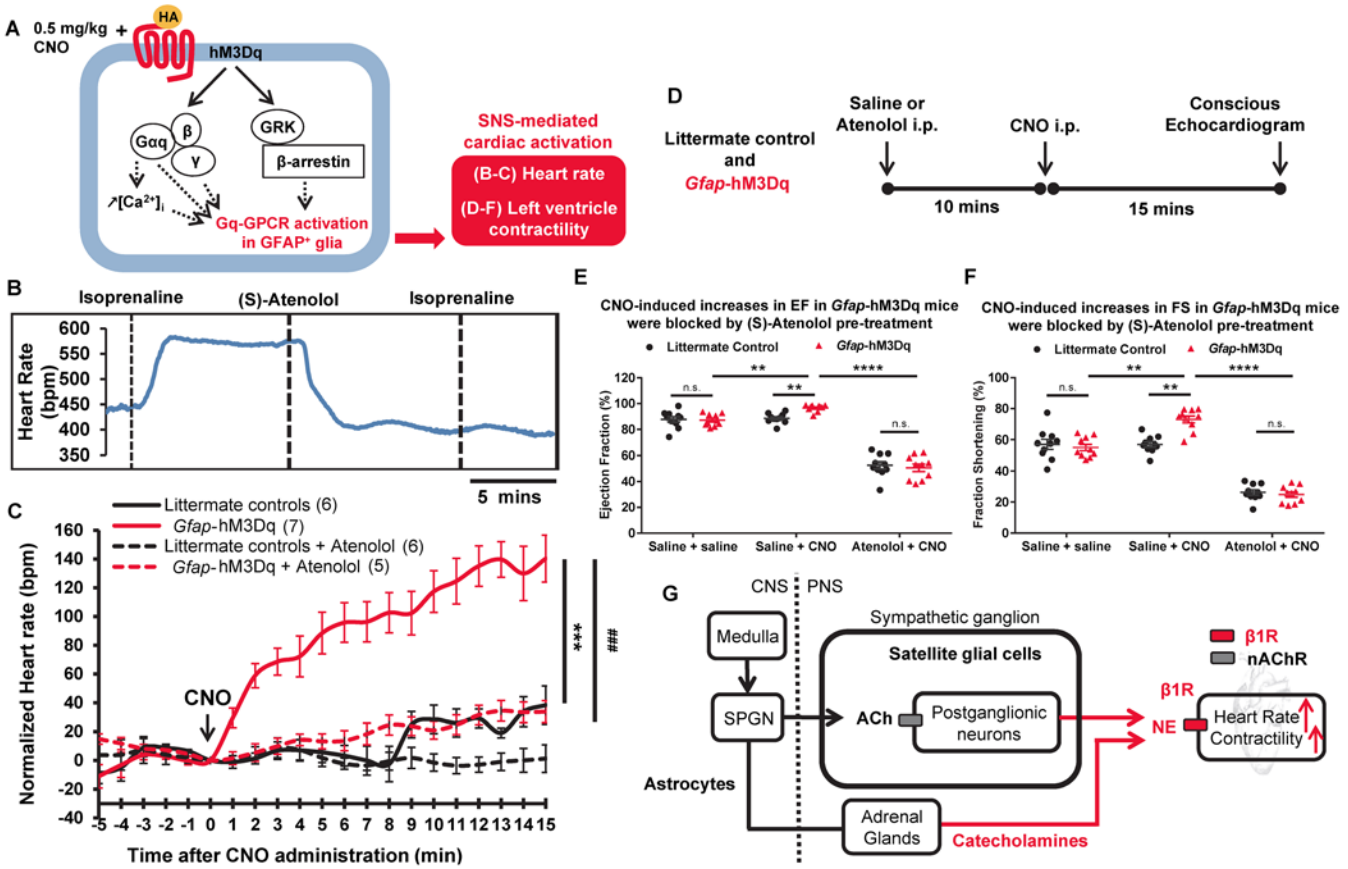

Figure 2. Acute activation of hM3Dq in GFAP⁺ glia led to robust, beta adrenergic receptor–mediated increases in heart rate and left ventricular contractility in *Gfap*-hM3Dq mice. (**A**) Schematic of in vivo model: CNO-induced hM3Dq activation in GFAP⁺ glia leads to changes in SNS-driven cardiovascular functions in *Gfap*-hM3Dq mice. (**B**) Heart rate recordings showed that 10 mg/kg (S)-atenolol blocked isoprenaline-induced increases in heart rate in C56BL/6J mice in vivo (6 recordings/2 mice). (**C**) CNO-induced significant increases in heart rate in *Gfap*-hM3Dq mice over 15 minutes compared with littermate controls (n = 5–7 mice in each group; 2-way ANOVA, $^{***}P < 0.0001$, time and genotype interaction between *Gfap*-hM3Dq and littermate controls), which were blocked by (S)-atenolol in vivo (2-way ANOVA, $^{\#\#\#}P < 0.0001$, time and treatment interaction between two *Gfap*-hM3Dq groups). Saline or atenolol were injected 10 minutes before CNO. (**D**) CNO-induced increases in left ventricle functions 15 minutes after CNO injections. Saline or atenolol was injected 10 minutes before CNO. (**E**) Significant increases in ejection fraction (EF) and (**F**) fraction shortening (FS) after CNO administration in *Gfap*-hM3Dq mice (unpaired t test; $^{**}P < 0.01$ between littermate control and *Gfap*-hM3Dq mice, also between two *Gfap*-hM3Dq groups; n = 10 for each genotype), which were blocked by (S)-atenolol pretreatment (unpaired t test; $^{****}P < 0.00001$ between the two *Gfap*-hM3Dq groups; n = 10 for each genotype). (**G**) Schematic model for potential mechanisms (red lines) underlying CNO-induced cardiac changes in vivo in *Gfap*-hM3Dq mice. nAChR, nicotinic acetylcholine receptors; SPGN, spinal preganglionic neurons.

hM3Dq-expressing medulla astrocytes in vivo. First, AAV8-DIO-GFAP-hM3Dq-mCherry (Vector Core at the University of North Carolina at Chapel Hill [UNC-CH]) was injected bilaterally into the medulla of *Gfap*-Cre mice (Supplemental Figure 3A). Mice were allowed to recover for 3 weeks before their heart rate responses to 0.5 mg/kg CNO were tested. By immunohistochemistry, mCherry was detected in nearly all medulla astrocytes (Supplemental Figure 3B), demonstrating that hM3Dq was expressed in the vast majority of medulla astrocytes. However, no change in heart rate was observed in viral vector–injected mice following injections with up to 2 mg/kg CNO (8 mice total, data not shown). Second, AAV8-DIO-GFAP-hM3Dq-mCherry was injected into the cisterna magna of *Gfap*-Cre mice in order to express hM3Dq in CNS astrocytes (33) (Supplemental Figure 3C). Three weeks after injection, mice were tested for CNO-induced heart rate changes in vivo (up to 2 mg/kg); no CNO-induced heart rate changes were detected in vivo (data not shown). These mice were then sacrificed to obtain acute brainstem slices. CNO-induced Ca^{2+} responses in medulla astrocytes were tested as a functional measure of hM3Dq expression in situ. More than half (~65%) of medulla astrocytes exhibited CNO-induced intracellular Ca^{2+} elevations (Supplemental Figure 3D), similar to the percentage of CNO-responding cells in *Gfap*-hM3Dq mice in situ (Figure 1E). Third, bolus-injections of CNO (0.5 mM, 20 μl) into cisterna magna of *Gfap*-hM3Dq mice (Supplemental

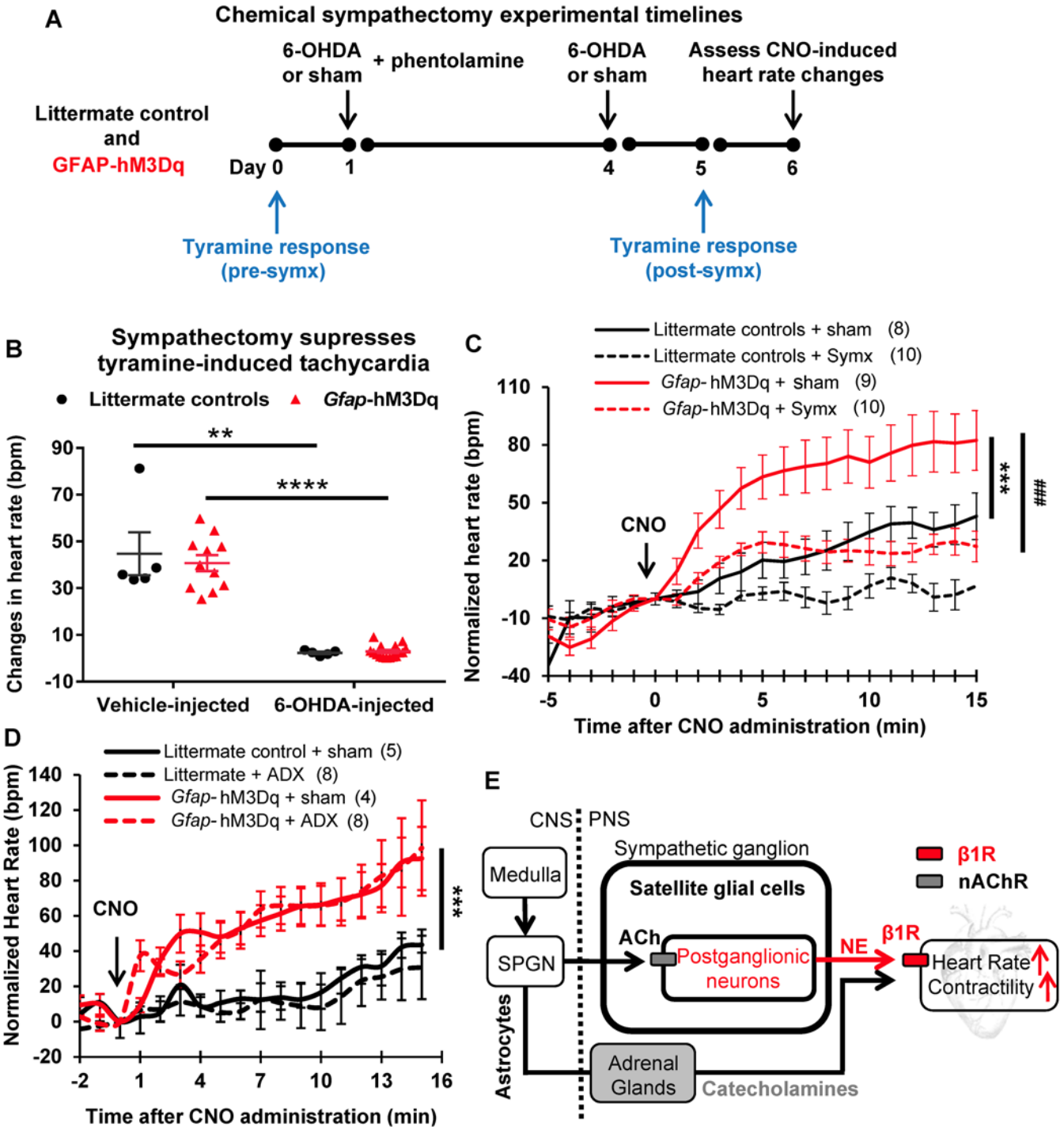

Figure 3. CNO-induced tachycardia is due to neural released NE, not adrenally released catecholamines. (**A**) Experimental timeline of 6-OHDA–induced chemical sympathectomy (symx). (**B**) Peripheral chemical sympathectomy largely suppressed tyramine-induced tachycardia in both littermate control mice (**P = 0.0017) and *Gfap*-hM3Dq mice (****P < 0.0001), indicating successful sympathectomy (unpaired t test; n = 5–16 for each group). (**C**) Peripheral chemical sympathectomy blocked CNO-induced tachycardia (n = 8–10 for each group; 2-way ANOVA, ***P = 0.0003, time and genotype interaction between vehicle-injected *Gfap*-hM3Dq mice and littermate controls; ###P < 0.0001, time and treatment interaction between vehicle- and 6-OHDA–injected *Gfap*-hM3Dq mice). (**D**) Bilateral adrenalectomy did not block CNO-induced changes in heart rate (n = 7–10 for each group; 2-way ANOVA, ***P < 0.0001, time and genotype interaction between vehicle-injected *Gfap*-hM3Dq mice and littermate controls). (**E**) Schematic model for CNO-induced, SNS-regulated cardiac changes in vivo in *Gfap*-hM3Dq mice. Red highlights the mechanism underlying CNO-induced changes in heart rate and left ventricle functions.

Figure 3F) also failed to increase heart rate (Supplemental Figure 3G). In summary, selective activation of hM3Dq-transduced brainstem astrocytes by CNO had no detectable effect on the heart rate in our experimental model. Therefore, activation of CNS GFAP$^+$ glia does not appear to be responsible for the cardiovascular phenotypes elicited by CNO in *Gfap*-hM3Dq mice.

Gq-GPCR activation in peripheral GFAP$^+$ cells is sufficient to increase heart rate and contractility in vivo. A new mouse model was developed to further validate the hypothesis that peripheral GFAP$^+$ glia rather than central GFAP$^+$ glia mediated the effects of CNO on heart rate in hM3Dq mice. In this model, *R26*-LSL-hM3Dq mice (34) were crossed with *P0*-Cre mice (35), a mouse line that exhibits Cre recombinase activity in peripheral glial cells including ganglionic SGCs. To validate this model, we crossed *P0*-Cre mice to a Cre reporter line (*Rosa26* flex switch OFP-L10a EGFP [TRAP] mice) (36) and examined recombination in *P0-Cre$^{+/-}$::TRAP$^{+/-}$* mice using immunocytochemistry. Findings from these experiments demonstrated that *P0*-Cre drives recombination primarily in the PNS. A small number of neurons in hippocampus, cortical regions, nuclei in the posteromedial hippocampal amygdala (AHiPM), and very few cerebellar Purkinje neurons (Figure 5A) exhibited recombination. No Cre recombination was observed in neurons in the brainstem (data not shown). Moreover, no Cre recombination was observed in GFAP$^+$ astrocytes, CNP$^+$ oligodendrocytes, or Iba-1$^+$ microglia in the brain (Figure 5B). In the sympathetic ganglia, Cre recombinase activity was detected in a subset of ganglionic SGCs as well as in myelinating Schwann cells (Figure 5C). Significant increases in heart rate were observed in *P0-Cre$^{+/-}$::hM3Dq$^{+/-}$* mice as compared with the littermate control *P0-Cre$^{-/-}$::hM3Dq$^{-/fl}$* mice following CNO injection (0.5 mg/kg, i.p.) (Figure 5D). These data further supported the hypothesis that the activation of Gq-GPCR signaling pathways in peripheral GFAP$^+$ glia leads to increases in heart rate. No CNO-induced changes in left ventricular contractility (EF or FS) were observed (Figure 5E).

Purinergic signaling between ganglionic SGCs and sympathetic neurons does not mediate CNO-induced increases in heart rate in vivo. Studies in sensory ganglia suggest potential purinergic signaling between SGCs and ganglionic neurons, which results in acute activation of neuronal activity (37). To test whether purinergic receptor activation is responsible for CNO-induced glial-neuronal interaction in sympathetic ganglia, we injected a nonselective P2 purinergic antagonist (PPADs) or a selective antagonist of P2X3 and P2X2/3 receptor (A-317491) into *Gfap*-hM3Dq mice 10 minutes prior to 0.5 mg/kg CNO administration. A-317491 did not abolish CNO-induced tachycardia in *Gfap*-hM3Dq mice in vivo (Figure 4F), suggesting that P2X3 receptor activation is unlikely to be the mechanism through which Gq-GPCR activation in SGCs regulates ganglionic neuronal activity. PPADs significantly suppressed but did not abolish CNO-induced tachycardia (Figure 4F), suggesting partial involvement of ATP. Moreover, we tested whether CNO-induced heart rate responses in vivo were altered in *Gfap*-hM3Dq mice crossed to *dnSNARE* mice (38) or *Cx43/Cx30* double knockout mice (39, 40). *dnSNARE* mice express the cytosolic portion of the SNARE domain of synaptobrevin 2 selectively in GFAP$^+$ glia (38) and have shown attenuated glial-driven purinergic currents in single cells isolated from brain slices (41). Cx43 hemichannels mediate Ca^{2+} responses in sensory SGCs (42) and contribute to the passage of ATP (43). The tachycardia elicited by CNO administration in both *Gfap-hM3Dq$^{+/-}$::Cx43$^{-/-}$/Cx30$^{-/-}$* mice and *Gfap-hM3Dq::dnSNARE::tTA* mice was comparable to that observed in *Gfap*-hM3Dq mice (Figure 4F). Accordingly, CNO-induced increases in ganglionic neuronal activity in vivo are unlikely to result from ATP release.

We next asked whether adenosine receptor activation is responsible for CNO-induced tachycardia in *Gfap*-hM3Dq mice. CNO administration (0.5 mg/kg) increased heart rate in *Gfap-hM3Dq::A1R$^{-/-}$* mice and *Gfap-hM3Dq::A2aR$^{-/-}$* mice (Figure 4F), suggesting that CNO-induced tachycardia is not mediated by A1R or A2aR activation. Administration of an adenosine A1R blocker (DPCPX, 1 mg/kg) 10 minutes prior to CNO administration also failed to block CNO-induced tachycardia in *Gfap*-hM3Dq mice in vivo (Figure 4F), further supporting the suggestion that adenosine receptor activation is not responsible for CNO-induced tachycardia.

Chronic activation of Gq-GPCR signaling in GFAP$^+$ glia leads to hypotension in female Gfap-hM3Dq mice. We next asked whether chronic CNO-induced Gq-GPCR activation in ganglionic SGCs leads to long-term changes in cardiac functions (Figure 6A). *Gfap*-hM3Dq mice and their littermate controls received CNO (0.5 mg/kg, i.p.) twice a day for 2 weeks; and their left ventricle functions and blood pressure were assessed between 2 and 3 days after the last CNO injection (Figure 6B). Chronic CNO administration resulted in a gradual decrease in body weight of *Gfap*-hM3Dq animals but not of littermate controls in both female and male animals (Figure 6C and Figure 7A, respectively); this effect could be due to increases in intestinal motility (15). Chronic CNO treatment resulted in hypotension in female *Gfap*-hM3Dq animals but not in littermate controls. The effect of

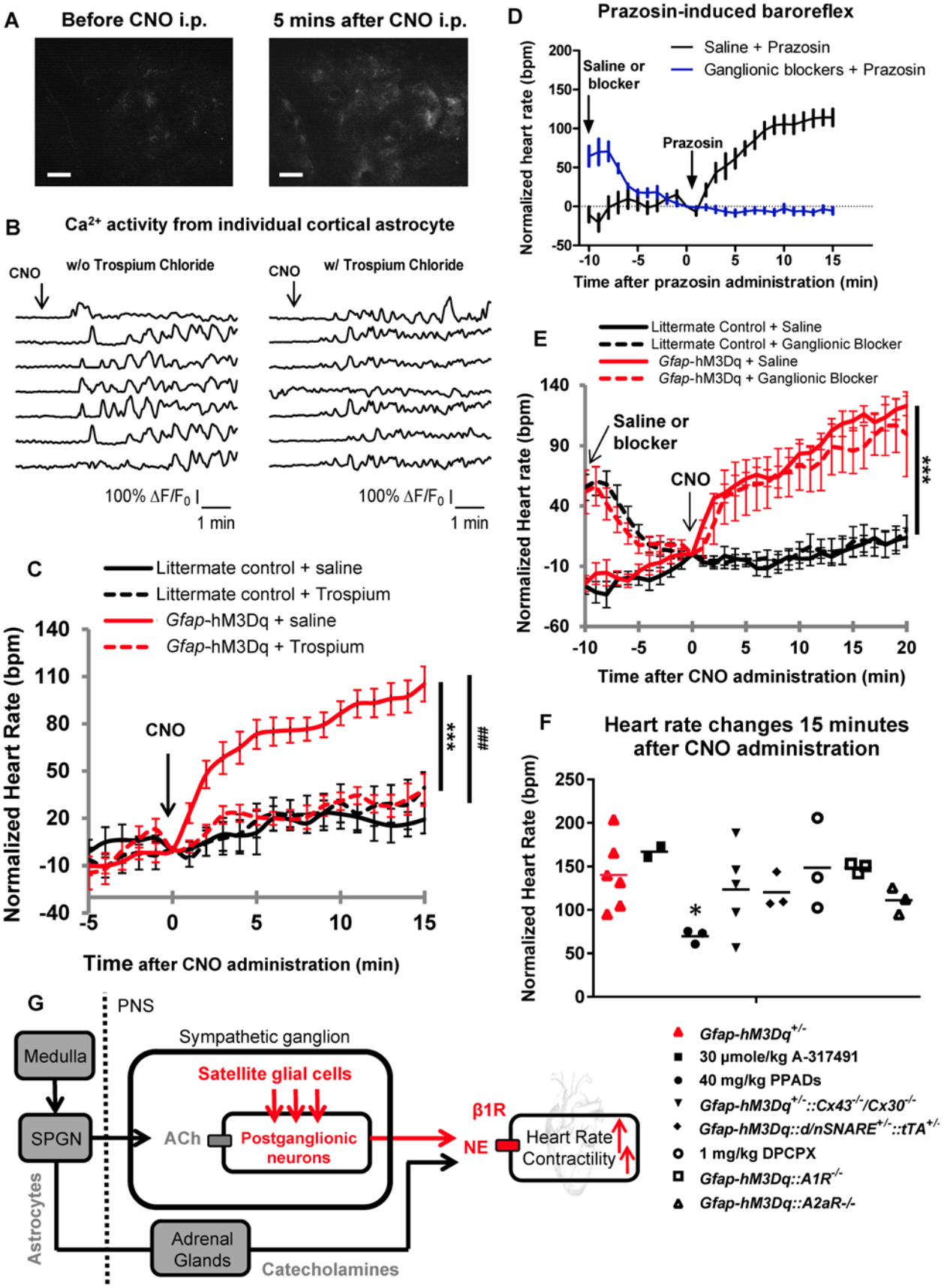
A
Before CNO i.p.
5 mins after CNO i.p.
B
Ca2+ activity from individual cortical astrocyte
CNO
w/o Trospium Chloride
w/ Trospium Chloride
100% ΔF/F0
1 min
C
Littermate control + saline
Littermate control + Trospium
Gfap-hM3Dq + saline
Gfap-hM3Dq + Trospium
Normalized Heart Rate (bpm)
CNO
***
###
Time after CNO administration (min)
D
Prazosin-induced baroreflex
Saline + Prazosin
Ganglionic blockers + Prazosin
Saline or blocker
Prazosin
Normalized heart rate (bpm)
Time after prazosin administration (min)
E
Littermate Control + Saline
Littermate Control + Ganglionic Blocker
Gfap-hM3Dq + Saline
Gfap-hM3Dq + Ganglionic Blocker
Saline or blocker
CNO
***
Normalized Heart rate (bpm)
Time after CNO administration (min)
F
Heart rate changes 15 minutes after CNO administration
Normalized Heart Rate (bpm)
Gfap-hM3Dq+/-
30 µmole/kg A-317491
40 mg/kg PPADs
Gfap-hM3Dq+/-::Cx43-/-/Cx30-/-
Gfap-hM3Dq::d/nSNARE+/-::tTA+/-
1 mg/kg DPCPX
Gfap-hM3Dq::A1R-/-
Gfap-hM3Dq::A2aR-/-
G
PNS
Medulla
SPGN
Sympathetic ganglion
Satellite glial cells
ACh
Postganglionic neurons
β1R
NE
Heart Rate
Contractility
Astrocytes
Adrenal Glands
Catecholamines

Figure 4. CNO-induced changes in cardiac functions are due to hM3Dq activation in peripheral glial cells, likely ganglionic SGCs. (**A**) AAV8-GFAP-GCaMP6–expressing astrocytes in visual cortex visualized through chronic polished window using 2-photon imaging before (left) and after (right) CNO i.p. injection in *Gfap*-hM3Dq mice (original magnification, 60×; scale bars: 40 μm). (**B**) Intracellular Ca^{2+} activity in cortical astrocytes in response to CNO i.p. administration, with or without i.p. trospium chloride injection (7 cells per condition, 2 repeats). (**C**) Trospium chloride, when administrated i.p., abolished CNO-induced increases in tachycardia (2-way ANOVA, n = 8–11 for each group; $^{***}P < 0.0001$, interaction between saline-treated *Gfap*-hM3Dq mice and littermate controls; $^{\#\#\#}P < 0.0001$, interaction between saline- and trospium-treated *Gfap*-hM3Dq mice). (**D**) A cocktail of ganglionic blockers decreased baseline heart rates and blocked prazosin-induced tachycardia in both *Gfap*-hM3Dq and littermate control mice (n = 8–9 for each group). (**E**) The cocktail of ganglionic blockers did not block CNO-induced tachycardia in *Gfap*-hM3Dq mice (2-way ANOVA, $^{***}P < 0.0001$, interaction between blocker-treated *Gfap*-hM3Dq mice and littermate controls, n = 8–10 for each group). (**F**) CNO administration (0.5 mg/kg, s.c.) led to increases in heart rate in *Gfap-hM3Dq*$^{+/-}$*::Cx43*$^{-/-}$*/Cx30*$^{-/-}$ mice (n = 6), *Gfap-hM3Dq*$^{+/-}$*::d/nSNARE*$^{+/-}$ mice (n = 3), *Gfap-hM3Dq*$^{+/-}$*::A1R*$^{-/-}$ mice (n = 3), and *Gfap-hM3Dq*$^{+/-}$*::A2aR*$^{-/-}$ mice (n = 3). Perturbing purinergic signaling with selective antagonists failed to block CNO-induced tachycardia in *Gfap*-hM3Dq mice; antagonists included P2X3 and P2X2/3 receptor antagonist (A-317491; n = 3) and adenosine A1 receptor antagonist (DPCPX; n = 3). Pre-block using nonselective P2 purinergic antagonist reduced but did not abolish CNO-induced tachycardia (PPADs; Mann-Whitney U test, $^{*}P < 0.01$, n = 3). (**G**) Schematic model for CNO-induced, SNS-regulated cardiac changes in vivo in *Gfap*-hM3Dq mice.

chronic CNO persisted well after cessation of CNO injections (Figure 6D), suggesting that overactivation of Gq-GPCR signaling in peripheral glia might contribute to cardiovascular dysfunction. Moreover, echocardiogram recordings revealed increased left ventricle diameter at the end of diastolic cycle in female *Gfap*-hM3Dq mice (Figure 6E) as compared with the female littermate controls, resulting in larger left ventricle volume at the end of diastolic cycles in CNO-treated female *Gfap*-hM3Dq mice (Figure 6F). These structure changes, however, did not result in significant changes in the left ventricle functions, including EF and FS (Figure 6, G and H, respectively) in female *Gfap*-hM3Dq mice. No significant enlargement of the left ventricle (data not shown) or changes in the weight of the heart were detected (Figure 6I). In contrast, chronic CNO treatment did not lead to significant changes in the blood pressure of male *Gfap*-hM3Dq mice (Figure 7B). No changes in left ventricle diameter (Figure 7C), volume at the end of the diastolic cycle (Figure 7D), left ventricle functions (Figure 7, E and F), or heart weight (Figure 7G) were observed in CNO-treated male animals.

Discussion

Glia-neuron interactions in the sympathetic ganglia. Our findings demonstrate that SGCs in the sympathetic ganglia are capable of regulating cardiac functions and blood pressure following their Gq-GPCR activation, suggesting a role for peripheral $GFAP^+$ glia in regulating cardiovascular functions. SGCs are the main type of glia in autonomic ganglia (44). In sympathetic and parasympathetic ganglia, SGCs form envelopes around individual neurons and synapses (44), creating a distinct functional unit consisting of a single ganglionic neuron and surrounding SGCs (45). SGCs express receptors for neurotransmitters (46, 47), potassium channels (48, 49), and neurotransmitter transporters (50, 51), suggesting active roles in controlling the chemical environment critical for neuronal activation. However, the ability of sympathetic SGCs to regulate ganglionic neuronal activity has never been directly tested, likely due to the inability to selectively activate SGCs without also activating neurons. To overcome this obstacle, we took advantage of DREADD technology and generated *Gfap*-hM3Dq transgenic mice (16).The engineered GPCR approach has been used by others to identify novel signaling pathways that play critical physiological roles in vivo (52–54). For example, Jain et al. used hM3Dq transgenic mice to demonstrate that Gq-GPCR signaling in pancreatic β cells led to activation of ERK1/2 and IRS2 signaling; this activation led to markedly improved β cell function (55). Recent studies where *Gfap*-hM3Dq was used to activate enteric glia revealed novel mechanisms of glial regulation of gastrointestinal functions (15, 56). In combination with pharmacological agents and by using in situ models, *Gfap*-hM3Dq mice serve as a useful model to study $GFAP^+$ glial functions in complex tissues and in intact animals.

How does SGC Gq-GPCR activation in the sympathetic ganglia lead to increases in cardiac activity? Our data suggest that it is likely due to direct activation of ganglionic neurons. Bidirectional purinergic signaling has been proposed to mediate sensory satellite glia-neuron interaction in the dorsal root ganglia via the activation of neuronal homomeric P2X3Rs and heteromeric P2X2/3Rs (57). In the sympathetic ganglia, P2XR expression is highly species- (58) and age-dependent (59). In our study, selective blockers for P2X3Rs and P2X2/3Rs failed to block CNO-induced tachycardia in *Gfap*-hM3Dq mice (Figure 4F), suggesting the lack of involvement of P2X3Rs in SGC-neuron interaction in the sympathetic ganglia following glial Gq-GPCR activation. However, PPADs showed a partial block effect on CNO-induced tachycardia (Figure 4F). This is consistent with previous report that in rat superior cervical ganglia, neurons respond to extracellular ATP mainly via P2YRs (47). Therefore, it is possible that CNO-induced SGC activation increases ganglionic neuronal activity via P2YR-mediated mechanisms.

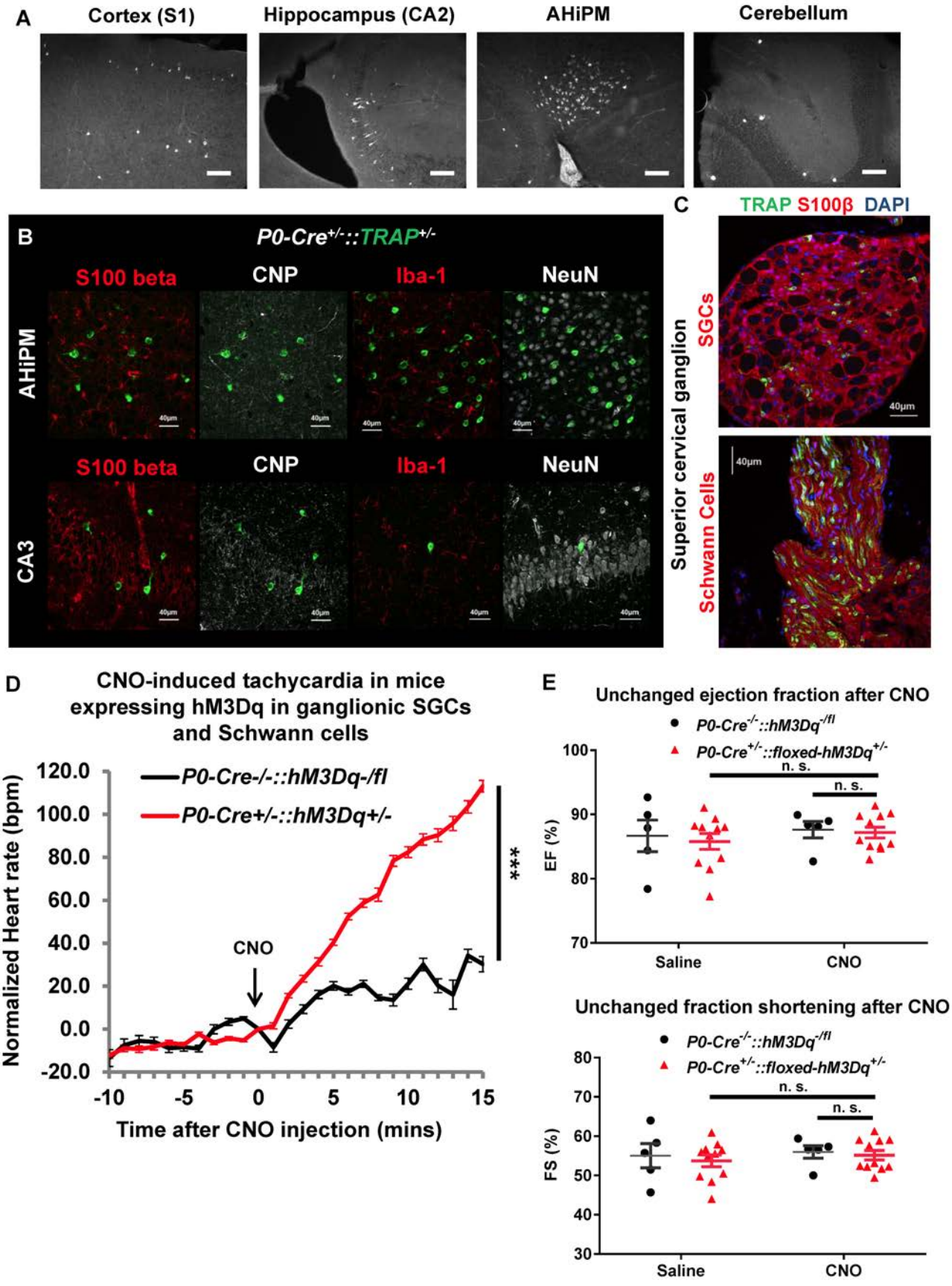

Figure 5. CNO administration increases heart rate in *P0-Cre*$^{+/-}$*::hM3Dq*$^{+/-}$ mice. (**A**) Cre recombinase activity can be detected in a very small subset of neuronal-like cells in the adult brain of *P0-Cre*$^{+/-}$*::TRAP*$^{+/-}$ mice (original magnification, 20×; scale bars: 100 μm). (**B**) Cre recombinase activity detected in AHiPM and hippocampus is restricted to neurons in the brain, and not detected in astrocytes, oligodendrocytes, or microglia. AHiPM, posteromedial hippocampal

amygdala. (**C**) A small subset of SGCs in the sympathetic ganglia also exhibit Cre recombinase activity in *P0*-Cre mice. Scale bars: 40 μm. (**D**) CNO administration (0.5 mg/kg, i.p.) led to increases in heart rate in *P0-Cre*$^{+/-}$*::hM3Dq*$^{+/-}$ mice but not in littermate control *floxed*-hM3Dq mice (2-way ANOVA, ***$P <$ 0.0001, *P0-Cre*$^{-/-}$*::hM3Dq*$^{-/fl}$, $n = 11$; *P0-Cre*$^{+/-}$*::hM3Dq*$^{+/-}$, $n = 15$). (**E**) CNO administration (0.5 mg/kg, i.p.) did not result in changes in left ventricular contractility in *P0-Cre*$^{+/-}$*::hM3Dq*$^{+/-}$ mice (unpaired *t* test, *P0-Cre*$^{-/-}$*::hM3Dq*$^{-/fl}$, $n = 5$; *P0-Cre*$^{+/-}$*::hM3Dq*$^{+/-}$, $n = 11$).

How does SGC Gq-GPCR activation activate neuronal P2YRs? It has been suggested that intracellular Ca^{2+} responses in GFAP$^+$ glia trigger ATP release via vesicular-dependent mechanism (11) or through Cx43 hemichannels (60). In our study, CNO-induced tachycardia persisted in mice lacking Cx43 and Cx30 (39, 40) as well as in mice expressing a dominant/negative mutation of synaptobrevin (d/nSNARE) in GFAP$^+$ glia (38), suggesting that SGC modulation of ganglionic neuronal activity does not involve the release of ATP through one of these mechanisms. On the other hand, SGCs can potentially regulate extracellular ATP concentration without directly releasing ATP. SGCs express enzymes for breaking down ATP (61, 62) and its metabolites (63, 64), which directly regulate neuronal excitability (46, 65, 66). Therefore, it is possible that Gq-GPCR activation in ganglionic SGCs modulates the concentration of extracellular ATP and in turn active neuronal P2YRs.

It has also been suggested that astrocytes release ATP that is rapidly converted to adenosine that then modulates neuronal activity through the activation of either A1 receptors (A1R) or A2a receptors (A2aR) (67, 68). Our study shows that CNO-induced tachycardia remains intact in *Gfap*-hM3Dq mice lacking A1R or A2aR (69, 70), suggesting that SGC Gq-GPCR activation–induced changes in ganglionic neuronal activity do not depend on adenosine receptor activation in neurons.

In addition to purinergic signaling, SGCs express much of the same machinery that CNS astrocytes utilize to regulate nearby neuronal and synaptic activity. Astrocytic Gq-GPCR activation potentiates glutamate and potassium (K^+) uptake (71), two key processes that regulate neuronal excitability. Sympathetic SGCs express inward rectifying potassium channels (Kir) (48, 72, 73) and glutamate transporters (74, 75). It is possible that SGC Gq-GPCR signaling regulates the excitability of postganglionic neurons via the modulation of these channels and transporters. Sympathetic SGCs also express GABA transporters (76, 77), which have been shown to regulate extracellular GABA concentration in a Ca^{2+}-dependent manner in astrocytes (78). These endogenous mechanisms can function independently of nicotinic ganglionic transmission, which is not responsible for the cardiovascular phenotypes induced by SGC Gq-GPCR activation in *Gfap*-hM3Dq mice (Figure 4E).

Peripheral versus central glial activation in sympathetic activation. CNO injections in *Gfap*-hM3Dq mice activate Gq-GPCR signaling pathways in CNS astrocytes and other peripheral GFAP$^+$ glia. Increasing cytoplasmic Ca^{2+} in brainstem astrocytes triggers robust respiratory responses (11) and increases SNA activity (12) in vivo. Therefore, we tested whether astrocytic Gq-GPCR activation contributed to observed phenotype in *Gfap*-hM3Dq mice. Pharmacogenetic activation of Gq-GPCR signaling and subsequent Ca^{2+} elevations in brainstem astrocytes did not increase heart rates in *Gfap*-hM3Dq mice (Supplemental Figure 3). These data are consistent with the lack of CNO-induced tachycardia when peripheral mACh antagonist was pre-administered (Figure 4C), or CNO-induced tachycardia in the presence of ganglionic blockers (Figure 4D).

As hM3Dq is also expressed in SGCs in the sensory ganglia, it is worth considering the possibility that sensory glial cells contribute to the observed phenotype. Activation of sensory SGCs positively regulates neuronal activity (79) and contributes to hyperalgesia and chronic pain (80–83). Sciatic nerve stimulation induces pressor responses and elicits tachycardia and blood pressure increase via SNS activation in rat (84, 85). However, unpublished findings in our laboratory indicate that CNO administration in *Gfap*-hM3Dq mice leads to a decrease in nociception and a reversal in inflammation-induced hyperalgesia; these phenotypes were abolished in *Gfap*-hM3Dq mice lacking A1R or A2aR (data not shown). These data further support the conclusion that sensory SGC activation is not responsible for CNO-induced SNS activation in *Gfap*-hM3Dq mice. Last, we considered the possibility that decreased sensory reflex leads to acute increases in SNS-induced functions. However, such somatosensory reflex requires ganglionic transmission (84, 85), which is not required for CNO-induced tachycardia (Figure 4E). Therefore, the activation of sensory SGCs does not appear to be responsible for CNO-induced cardiac phenotypes in *Gfap*-hM3Dq mice.

It is also possible that hM3Dq is expressed in GFAP$^+$ type II cells in the carotid bodies (86, 87) and that these cells modulate the activity of type I neurons via bidirectional purinergic signaling (88). Type I neuron depolarization could lead to CNS-mediated chemoreflexes, including hyperventilation, sympathoexcitation and increases in blood pressure (89). However, just like somatosensory reflex, these central actions require

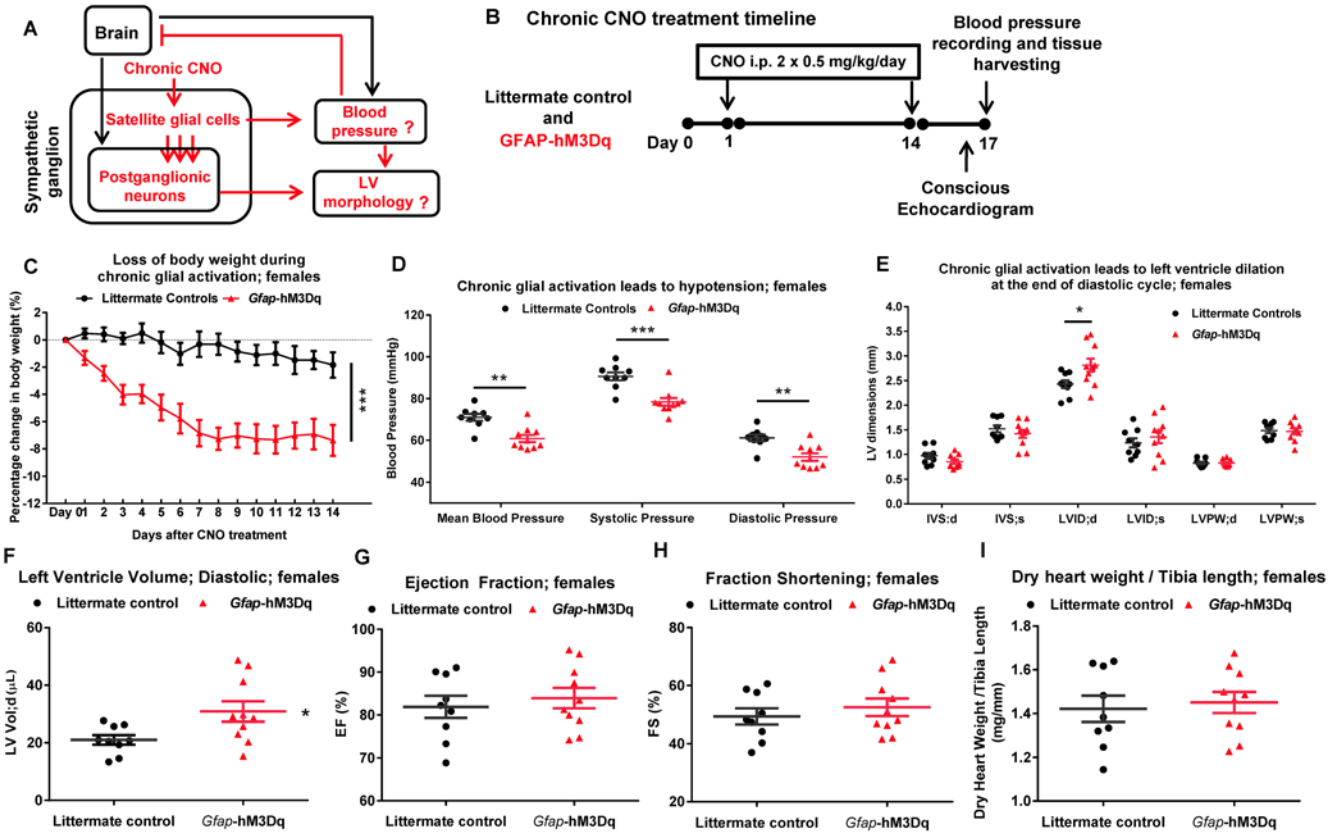

Figure 6. Chronic glial activation leads to hypotension and left ventricle dilation in female *Gfap*-hM3Dq mice. Littermate controls, $n = 9$; *Gfap*-hM3Dq, $n = 10$ throughout the figure. (**A**) Schematic model for chronic activation of ganglionic SGCs and potential cardiovascular outcomes. (**B**) Chronic CNO treatment experiment timeline. (**C**) Chronic CNO-induced glial activation led to a significant decrease in body weight in female *Gfap*-hM3Dq mice but not female littermate controls at the end of the treatment period (2-way ANOVA, $^{***}P < 0.0001$, time and genotype interaction). (**D**) Chronic CNO-induced glial activation led to hypotension in female *Gfap*-h3Dq animals relative to littermate controls (Mann-Whitney *U* test, $^{**}P < 0.01$, $^{***}P < 0.001$). (**E**) Echocardiogram recordings showed that chronic CNO treatment led to increased left ventricle diameter at the end of the diastolic cycle (left ventricular internal diameter end diastole [LVID;d]) in female *Gfap*-hM3Dq mice compared with female littermate controls (Mann-Whitney *U* test, $P < 0.05$). IVS;d and IVS;s, interventricular septal end diastole and end systole. LVPW;d and LVPW;s, left ventricular posterior wall end diastole and end systole. (**F**) The volume of the left ventricle at the end of diastolic cycle was significantly increased in female *Gfap*-hM3Dq mice after 2 weeks of CNO treatment (Mann-Whitney *U* test, $^{*}P < 0.05$). (**G** and **H**) Chronic CNO treatment did not result in changes in ejection fraction (**G**) or fraction shortening (**H**) in female *Gfap*-hM3Dq animals compared with littermate controls (Mann-Whitney *U* test). (**I**) The weight of the hearts of female *Gfap*-hM3Dq animals did not change after chronic CNO treatment (Mann-Whitney *U* test).

nicotinic ganglionic transmission. In *Gfap*-hM3Dq mice, blocking nicotinic ganglionic transmission did not suppress CNO-induced tachycardia, suggesting that the activation of neuronal activity in carotid bodies is not responsible for CNO-induced SNS activation in *Gfap*-hM3Dq mice. Overall, our findings strongly suggest that Gq-GPCR activation in sympathetic SGCs positively regulates SNS-regulated heart functions.

To directly test the hypothesis that SGCs in the sympathetic ganglia mediated the observed cardiovascular effect, we restricted hM3Dq expression to SGCs and Schwann cells by crossing *P0*-Cre transgenic mice (90) with $hM3Dq^{-/fl}$ mice. $P0\text{-}Cre^{+/-}::hM3Dq^{+/-}$ mice did not exhibit a CNO-induced increase in left ventricular contractility. This may be because of the low percentage of recombination in SGCs in the sympathetic ganglia in $P0\text{-}Cre^{+/-}$ mice. Thus, the effect mediated by SGC Gq-GPCR activation on left ventricular contractility is less pronounced in $P0\text{-}Cre^{+/-}::hM3Dq^{+/-}$ mice. However, during heart rate recordings, $P0\text{-}Cre^{+/-}::hM3Dq^{+/-}$ mice were subjected to 1.5% isoflurane, and their heart rates were decreased by ~20% compared with unanesthetized mice. Isoflurane anesthesia generally decreases sympathetic nerve activity to target organs (91), which may have contributed to the more profound influence of CNO-induced sympathetic activation on heart rate.

Do satellite glia play a role in neurogenic CVDs? SGCs exhibit changes during aging (92) and in response to sympathetic overactivation (93). In rat superior cervical ganglia, both preganglionic electrical stimulation and beta adrenergic receptor agonist administration induce cAMP synthesis in SGCs (93). In these studies the

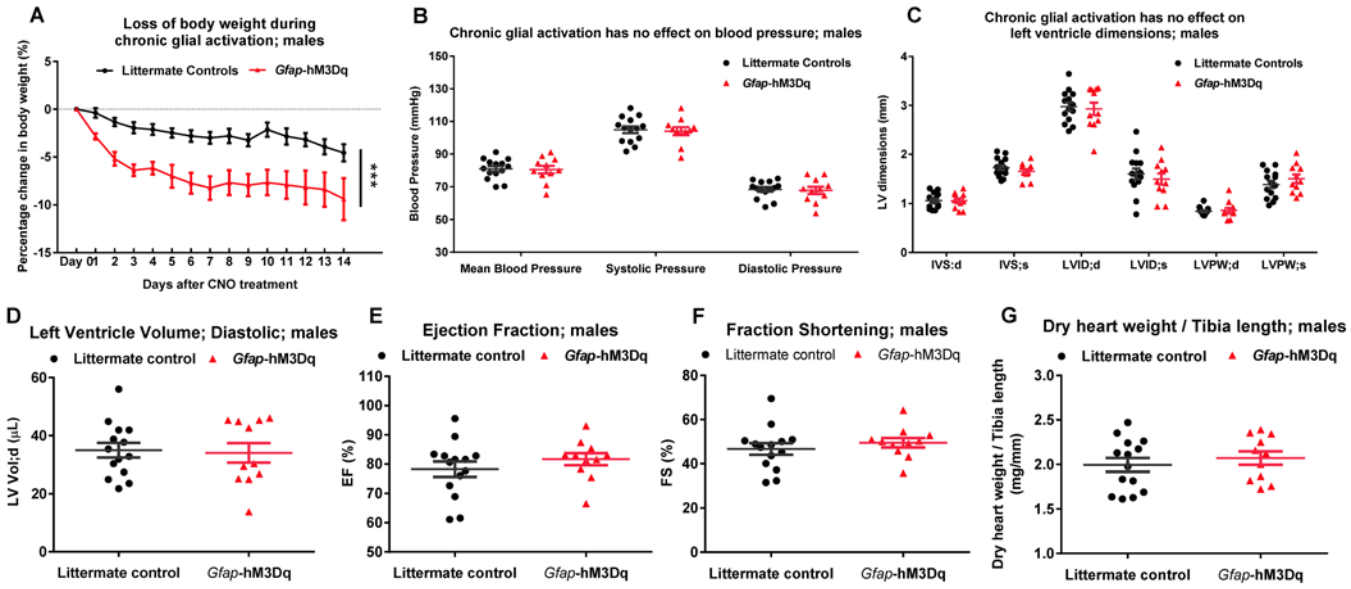

Figure 7. Chronic CNO treatment in male *Gfap*-hM3Dq mice did not lead to changes in cardiovascular phenotypes as observed in CNO-treated female *Gfap*-hM3Dq mice. Littermate controls, $n = 14$; *Gfap*-hM3Dq, $n = 11$ throughout the figure. (**A**) Chronic CNO treatment led to a decrease in the body weight of male *Gfap*-hM3Dq mice (2-way ANOVA, $^{***}P < 0.0001$). (**B**) In contrast to what was observed in female *Gfap*-hM3Dq animals, chronic CNO treatment did not induce hypotension in male *Gfap*-hM3Dq mice (Mann-Whitney *U* test). (**C** and **D**) In contrast to what was observed in female *Gfap*-hM3Dq mice, chronic CNO treatment did not induce changes in left ventricle diameter (**C**) or volume (**D**) at the end of the diastolic cycle (Mann-Whitney *U* test). (**E** and **F**) Left ventricle functions did not change after chronic CNO treatment in male *Gfap*-hM3Dq mice compared with their littermate controls (Mann-Whitney *U* test). (**G**) Chronic CNO treatment in male *Gfap*-hM3Dq mice did not lead to changes in heart weight when normalized to tibia length (Mann-Whitney *U* test).

accumulation of cAMP in SGCs was much greater in stroke-prone rat strains (SHR) compared with normal rat strains (Sprague-Dawley and Wistar Kyoto [WKY]) (94), suggesting a possible link between signaling events in SGCs and the risk of CVD. However, the causative link between SGC activation and abnormalities in cardiovascular outcomes has not been directly explored. We asked whether selective activation of Gq-GPCR signaling in SNS glia but not neurons led to changes in cardiovascular function. Chronic CNO administration led to hypotension and significant increases in left ventricle diameter and volume at the end of the diastolic cycles in female *Gfap*-hM3Dq mice (Figure 6); these findings suggest that glial activation alone plays an important role in long-term sympathetic control of heart and vessel function. Despite acute increases in blood pressure in response to a single i.p. injection of CNO in *Gfap*-hM3Dq mice (16), chronic glial activation induced hypotension in female *Gfap*-hM3Dq mice (Figure 6). This could be attributed to homeostatic changes in the central set-point for blood pressure in response to increases in blood pressure via peripheral feedback. In humans, hypertensive females, but not hypertensive males, show a significant reduction in baroreceptor reflex sensitivity with age while sympathetic tone increases (95). In addition, the hypotension phenotype we observed also could be occurring at the expense of left ventricle dilation (Figure 6) and possible changes in blood volume. Although it is well know that there are sex differences in sympathetic activity, blood pressure regulation (96–98), and CVDs (97), the majority of the animal studies of cardiovascular regulation and disease use male animals exclusively. Our data suggest that females may exhibit greater homeostatic regulation on blood pressure in response to increased blood pressure compared with their male counterparts. We aim in the future to explore the sex differences in glial-induced blood pressure regulation in our future studies.

Sympathetic overactivation is known to cause tachycardia, left ventricular dysfunction and hypertrophy, neurogenic hypertension, and insulin resistance (6). Our findings suggest that ganglionic SGCs might serve as a target in the peripheral system for manipulating heart and blood vessel function. SGCs in the sensory ganglia have been targeted for adenoviral gene therapy in animal models of chronic pain (99–101). In humans, injections into sympathetic ganglia are commonly performed without major side effects (102–104). Based on our study, SGCs Gq-GPCR signaling may offer strong therapeutic potential for suppressing sympathetic overactivation in treating neurogenic CVDs.

Methods

Animals

Gfap-hM3Dq mice (16) (Figure 1A) were maintained on a C57BL/6J background, and all tests were performed on N11 to N15 generational backcrossed mice. In all experiments, hM3Dq-negative littermates were used as controls. For Ca^{2+} imaging experiments, *Gfap*-hM3Dq mice were crossed to *Gfap*-GCaMP3 mice to generate *Gfap-hM3Dq*$^{+/-}$*::Gfap-GCaMP3*$^{+/-}$ mice.

Gfap-GCaMP3 mice were generated as follows: the coding sequence for GCaMP3 (105) (a gift from L. Looger; Addgene, plasmid 22692) was cloned into the plasmid pTg1 (courtesy of R. Thresher, UNC-CH) upstream of the post-translational enhancer sequence from the woodchuck hepatitis virus (WPRE) and poly(A) sequence from SV40. The 2.2-kb human GFAP promoter from pGfa2Lac1 (courtesy of M. Brenner, University of Alabama at Birmingham, Birmingham, Alabama, USA) was placed upstream of the intron-GCaMP3-WPRE-pA sequence in pTg1 (Supplemental Figure 2A). This DNA construct was then injected into C57BL/6J embryos by the Animal Models Core Facility at UNC-CH. *Gfap*-GCaMP3 mice were backcrossed to C57BL/6J mice for at least 5 generations before being used in experiments or bred to *Gfap*-hM3Dq mice.

Gfap-Cre mice were obtained from the Jackson Laboratory (JAX; stock no. 024098). *Glt1*-eGFP mice (106) (GLT1: EAAT2, slc1a2, a glutamate transporter) were obtained from J.D. Rothstein (Johns Hopkins University, Baltimore, Maryland, USA).

P0-Cre (*P0*: myelin protein zero) (90) mice were obtained from JAX(stock no. 017927) and bred to *R26*-LSL-hM3Dq mice (34) (gift from B.L. Roth, UNC-CH). *P0*-Cre mice were also bred to *Rosa26* flex switch OFP-L10a EGFP (TRAP) mice (36) (gift from M.G. Caron, Duke University, Durham, North Carolina, USA) to verify the Cre-expressing population.

Mice that conditionally express a dominant-negative domain of vesicular SNARE VAMP2/synaptobrevin2 (d/nSNARE) under the control of the GFAP promoter were generated by crossing *Gfap*-tTA transgenic mice (107) and *tetO*-d/nSNARE mice (38). Mice lacking Cx43 and Cx30 were obtained by breeding *Gfap*-Cre mice with *Cx43*$^{fl/fl}$*::Cx30*$^{-/-}$ mice (39, 40), resulting in deletion of Cx43 in cells of the GFAP$^+$ cells and global deletion of Cx30. Mice lacking A1R (*A1R*$^{-/-}$ mice; ref. 69) and A2aR (*A2aR*$^{-/-}$ mice; ref. 70) were a gift from S. Tilley (UNC-CH). These mouse lines were bred separately with *Gfap-hM3Dq*$^{+/-}$ mice, resulting in hM3Dq expression in GFAP$^+$ cells in either *A1R*$^{-/-}$ mice or *A2aR*$^{-/-}$ mice.

All transgenic mice were generated and maintained in the C57BL/6J background. Both sexes were balanced in all experiments. Mice were maintained in a temperature-controlled environment in the animal facilities at the UNC-CH on a reversed 12-hour light/12-hour dark cycle, with ad libitum access to food and water. Experiments took place during the dark cycle.

In vivo measurements for cardiovascular functions

All cardiovascular measurements were performed during the active/dark period (between 8 am and 6 pm). Noninvasive recordings of heart rate and pulse distention were measured with a MouseOx pulse oximeter (Starr Life Science) under 1.5% isoflurane (Piramal Healthcare) anesthesia while body temperature of the mice was maintained at 37°C. Conscious echocardiography was performed by the UNC Animal Surgery Core Lab using Vevo 2100 (VisualSonics). Common parameters for left ventricular functions such as ventricle wall thickness, EF, and FS were analyzed using Vevo 2100 version 1.6.0. In all in vivo experiments, saline or 0.5 mg/kg CNO was administered via intraperitoneal injection (100 µl/25g BW, i.p.) or subcutaneous injection (25 µl/25 g BW, s.c.) depending on the body position of the animal. Experiments were terminated 15 minutes after CNO injections unless otherwise indicated. Investigators were blinded to the genotype during experiments and analysis of the experimental outcome.

Pharmacogenetic and pharmacological manipulations

CNO (powder form, provided by the NIH through B.L. Roth) was dissolved in DMSO at 1 mg/ml and then diluted in physiological saline for s.c. and i.p injections (0.125% final DMSO concentration). For chronic CNO treatment, animals received i.p. injections of 0.5 mg/kg CNO (diluted in physiological saline, with 0.125% DMSO) twice a day, 4 hours apart during their active period (108). Pharmacological agents used in this study and their working concentrations are provided in Table 1.

Heart weight

After assessment of heart functions at the end of chronic CNO administration, mice were sacrificed and

Table 1. Chemicals used in pharmacological experiments

Reagent	Vendor/source	Catalog no.	Working concentration
Clozapine N-oxide (CNO)	NIH, Roth lab	N/A	0.5 mg/kg
(S)-(-)-atenolol	Sigma-Aldrich	A143	10 mg/kg
Isoprenaline hydrochloride	Sigma-Aldrich	I5627	0.1 mg/kg
Corticosterone	Sigma-Aldrich	27840	25 mg/l
6-Hydroxydopamine hydrobromide (6-OHDA)	Sigma-Aldrich	16297	150 mg/kg
Phentolamine hydrochloride	Sigma-Aldrich	P7547	150 μg/kg
Tyramine hydrochloride	Sigma-Aldrich	T2879	100 μg/kg
Trospium chloride	Toronto Research Chemicals	T892800	20 mg/kg
Prazosin hydrochloride	Sigma-Aldrich	P7791	1 mg/kg
Hexamethonium chloride	Sigma-Aldrich	H2138	20 mg/kg
Chlorprothixene hydrochloride	Sigma-Aldrich	C1671	5 mg/kg
A-317491 sodium salt hydrate	Sigma-Aldrich	A2979	30 μmol/kg
PPADS tetrasodium salt 7H2O	Tocris Bioscience	0625	40 mg/kg
DPCPX	Tocris bioscience	0439	1 mg/kg

Roth lab, laboratory of Bryan L. Roth, UNC-CH

their hearts and tibiae isolated using standard methods. Tissues were rinsed in cold 1× PBS 3 times to remove blood. Hearts and tibiae were then left in a dry oven (80°C) overnight. The dry weight of the hearts and dry length of the tibiae were recorded in the morning of the following day. Investigators were blinded to the genotype during the measurements.

Chemical sympathectomy

Chemical sympathectomy was performed by two 6-OHDA (150 mg/kg in 0.1% ascorbic acid, i.p.) injections 3 days apart (27) to trigger sympathetic denervation in peripheral organs including heart. The alpha adrenergic receptor blocker phentolamine (150 μg/kg, i.p.) was injected with the first 6-OHDA injection to protect animals from massive release of catecholamines associated with 6-OHDA administration (27). Vehicle-injected *Gfap*-hM3Dq and littermate control animals received two 0.1% ascorbic acid injections and a phentolamine injection. The effectiveness of sympathectomy was determined by assessing tyramine-induced (100 μg/kg, i.v.) tachycardia before and after chemical sympathectomy. Effective chemical sympathectomy was defined as an 85% or greater suppression of tyramine-induced tachycardia (27, 29). Cardiovascular in vivo measurements were performed 24 hours after the second 6-OHDA injection (27).

ADX

ADX surgeries were performed as described by M. van den Buuse et al. (109). In brief, anesthetized mice (1.5% isoflurane) were placed in ventral recumbency. A 1-cm dorsal midline incision was made with its midpoint centered over the last rib. The muscle wall on either side of the spinal column was pierced with blunt forceps; the adrenal glands were located, then removed. Skin incisions were closed with liquid suture and stainless steel wound clips. Sham-operated animals went through the same manipulation except their adrenal glands were manipulated and left intact. Carprofen (5–10 mg/kg) was administered s.c. for 3 days after surgery. Adrenalectomized mice were maintained with ad libitum 0.9% sodium chloride drinking water containing 25 mg/l corticosterone and 0.2% EtOH (to dilute corticosteroid) (109), whereas sham-operated mice received regular drinking water containing 0.2% EtOH.

Viral expression of hM3Dq

AAV8-DIO-GFAP-hM3Dq-mCherry injections into brainstem. AAV8-DIO-GFAP-hM3Dq-mCherry (3×10^{13} virus molecules/ml, 1.5 μl) was bilaterally injected into the medulla of *Gfap*-Cre mice. The medulla was located using stereotaxic coordinates: from the bregma –6.74 ± 0.1 mm caudal, 1.4 ± 0.1 mm lateral, and 5.7 mm ventral. This was accomplished using a rodent stereotaxic frame fitted with an isoflurane gas mask adaptor for mice (Kopf). The expression of hM3Dq in medulla astrocytes was later confirmed by increases in $[Ca^{2+}]_i$ in response to bath CNO application in acute brain slice preparation, or by overlapping mCherry and GFAP immunoactivity in brainstem tissues. After adeno-associated virus (AAV) injection, mice were

allowed to recover for at least 3 weeks before being used in experiments.

Central CNO delivery via injection of cisterna magna (ICM) during in vivo cardiovascular recording. CNO was dissolved in a small volume of DMSO and further diluted in artificial cerebrospinal fluid (ACSF) (21) to a final concentration of 0.5 mM. After 5 minutes of stable baseline of cardiovascular recordings using the STARR system, the recordings were paused, and 20 μl CNO was injected as a bolus into the cisterna magna. This was accomplished by lowering a 30-gauge needle approximately 1 mm into the cisterna magna at an angle of 45 degrees while maintaining isoflurane anesthesia. An equal volume of DMSO/ACSF was used as a control solution. After injection, the needle was retracted, and the cardiovascular recordings were immediately resumed. This procedure was used to deliver AAV into the CSF; injection of dyes using this procedure leads to staining in most regions of CNS (110, 111).

In situ brainstem slice preparation and Ca^{2+} imaging

Acute mouse brainstem slices were prepared from P20–P30 mice. Briefly, mice were anesthetized using isoflurane and decapitated. 350-μm coronal slices were cut using a Leica VT1000 vibratome in ice-cold, nominally Ca^{2+}-free cutting buffer (21). Slices were incubated for 45 minutes at 35°C in low-Ca^{2+} ACSF (21). SR-101 (1 μM, Sigma-Aldrich) was added into the low-Ca^{2+} ACSF for the first 30 minutes to label astrocytes. Slices were then transferred and kept in 3 mM [K^+] ACSF at room temperature (21). Experiments were conducted in the standard ACSF at room temperature. All solutions were continuously aerated with 95% O_2/5% CO_2.

All of the Ca^{2+} imaging experiments were performed on a confocal microscope equipped with a 643-RYB-A02 S/N 1045 laser (Melles Griot) and a 60×, 0.9 NA objective. GCaMP3 and SR-101 signals were collected simultaneously in all the recordings. Field recordings were performed to detect Ca^{2+} activity in brainstem astrocyte processes at a frame rate of 1.1 seconds (0.9 Hz). FluoView was used for image analysis and to analyze Ca^{2+} dynamics from cell soma. Ca^{2+} responses were defined as fluxes at least 2 standard deviations above the averaged 30-second baseline value.

Superior cervical ganglia explant cultures and Ca^{2+} imaging

Primary cultures of sympathetic ganglia explants were prepared from P30–P45 mice. In brief, mice were sacrificed by isoflurane overdose and decapitated. Superior cervical ganglia were dissected out and treated with collagenase (1 mg/ml) for 20 minutes at 37°C. The ganglia were then plated on collagen-coated glass slides in medium containing 50 ng/ml 2.5S NGF, 10% FCS, 2 mM glutamine, and 100 mg/ml penicillin in Eagle's minimum essential medium with Earle's salts (Life Technologies Inc.). Ganglia were allowed to attach and grow on coverslips for at least 5 days before experiments. Images were collected using the same setup and software as those used for in situ brainstem slice preparation.

AAV injection for expression of GCaMP6 and 2-photon imaging through polished, reinforced thinned-skull optical windows

P45–P90 *Gfap*-hM3Dq mice were anesthetized with 1.5% isoflurane, and a vertical incision was made over one side of the primary visual cortex. A glass pipette containing AAV8-GFAP-*Lck*-GCaMP6s (1.5×10^{12}) was lowered through thinned skull into visual cortex, and AAV was injected using a Harvard Apparatus 11 Plus pump and a syringe-to-pipette coupling system. The incision was sealed with Vetbond and a surgical staple, covered with antibiotic ointment. The mice were given a single injection of antibiotic s.c. (ciprofloxacin, 5 mg/kg body weight) and allowed to recover for 4 weeks. Polished, reinforced thinned-skull (PoRTS) optical windows were prepared as previously described (31), and mice were allowed to recover for 5 days. Using a PoRTS optical window, Ca^{2+} activity in cortical astrocytes at 200- to 250-μm depth can be imaged multiple times over several weeks (31). A custom 2-photon microscope, converted from an Olympus Fluoview 300 system, with a 60×, 0.9 NA water-immersion objective and Hamamatsu photomultiplier tubes, was used for imaging. Images were acquired using Fluoview 300 software at 1–2 Hz.

Immunohistochemistry

Immunohistochemistry staining was performed according to standard protocols. Superior cervical ganglia, hearts, or brain tissues were harvested from mice perfused with ice-cold 4% PFA, and samples were post-fixed in 4% PFA at 4°C overnight. After cryoprotection, all samples were frozen and cut to 20-μm sections on a cryostat or a Leica SM2010R microtome. Blocking solution contained 10% donkey serum and 0.05% Triton X-100 (brain slices) or 0.2% Triton X-100 (peripheral tissues) in 1× PBS. Primary antibodies used

Table 2. Primary and secondary antibodies used

Antibody	Vendor	Catalog no.	Dilution
Goat anti-GFP	Rockland	600-101-215	1:1,000
Mouse anti–tyrosine hydroxylase	Sigma-Aldrich	T1299	1:500
Rabbit anti–brain lipid binding protein (BLBP)	Millipore	ABN14	1:500
Rabbit anti–S100 beta	Abcam	ab52642	1:500
Mouse anti-CNPase	Millipore	MAB326	1:500
Rabbit anti–iba-1	Wako	019-19741	1:1,000
Mouse anti-NeuN	Sigma-Aldrich	MAB377	1:500
DAPI	Invitrogen	D1306	1:250

are listed in Table 2. Alexa Fluor secondary antibodies (1:500) were purchased from Invitrogen. Stained sections were viewed with a 40× or 60× oil objective on an Olympus confocal microscope using FluoView.

Statistics

For all heart rate recordings, data were collected at 15 Hz and averaged using 1-minute bins. To control for the variability of baseline heart rates, each animal's heart rates were normalized to their baseline heart rate, which was calculated from the whole minute before CNO injection. Normalized heart rates (Δ heart rate) were then presented over time. All data are presented as mean ± SEM. Data were analyzed using either unpaired *t* test or 2-way ANOVA with genotype and treatment as between-subject factors. When appropriate, individual parameters of data were compared using 2-tailed *t* test analysis. For all comparisons, an α of 0.05 was selected (*).

Study approval

All mice were housed and all experimental procedures performed according to protocols approved by the Institutional Animal Care and Use Committee of UNC-CH.

Author contributions

AXX and KDM designed the study and wrote the manuscript; AXX and JJL performed the experiments and analyzed data. All authors reviewed the manuscript.

Acknowledgment

We thank Patrice G. Guyenet (University of Virginia) for comments on this manuscript; Kristen M. Boyt (McCarthy laboratory, UNC-CH) for generating and characterizing *Gfap*-hM3Dq mice as well as for comments on this manuscript; Brian C. Cooley and Sean T. Hick of the MHI Animal Surgery Core Laboratory at UNC-CH for performing cardiovascular recordings; Molly Cook for performing viral injections into medulla; Seth D. Depuy (Eli Lilly and Co.) for training in preparing and recording acute brainstem slices; Mohanish Deshmukh (UNC-CH) and Ryan Annis (Deshmukh laboratory, UNC-CH) for the training of ganglia dissection and explant culture; Lan Mao (H.A. Rockman laboratory, Duke University) for the training of adrenalectomy; David Reich (Brown University) for help with immunostaining in explant culture. The work in the McCarthy laboratory is supported by NIH R21-NS081589-01.

Address correspondence to: Alison Xiaoqiao Xie, Department of Pharmacology, 120 Mason Farm Road, CB # 7365, 4049 Genetic Medicine, Chapel Hill, North Carolina 27599-7365, USA. Phone: 919.966.1152; E-mail: alisonxie@unc.edu.

JJL's present address is: School of Medicine, University of South Carolina, Columbia, South Carolina, USA.

1. Thomas GD. Neural control of the circulation. *Adv Physiol Educ*. 2011;35(1):28–32.
2. Guyenet PG. The sympathetic control of blood pressure. *Nat Rev Neurosci*. 2006;7(5):335–346.
3. Kaye DM, Esler MD. Autonomic control of the aging heart. *Neuromolecular Med*. 2008;10(3):179–186.
4. Malpas SC. Sympathetic nervous system overactivity and its role in the development of cardiovascular disease. *Physiol Rev*. 2010;90(2):513–557.
5. Schlaich MP, et al. Sympathetic augmentation in hypertension: role of nerve firing, norepinephrine reuptake, and angiotensin neuromodulation. *Hypertension*. 2004;43(2):169–175.

6. Grassi G, Seravalle G, Quarti-Trevano F. The 'neuroadrenergic hypothesis' in hypertension: current evidence. *Exp Physiol*. 2010;95(5):581–586.
7. Schwartz PJ. Cardiac sympathetic denervation to prevent life-threatening arrhythmias. *Nat Rev Cardiol*. 2014;11(6):346–353.
8. Zhao Q, et al. Effects of intrinsic and extrinsic cardiac nerves on atrial arrhythmia in experimental pulmonary artery hypertension. *Hypertension*. 2015;66(5):1042–1049.
9. Kasama S, et al. Prognostic value of cardiac sympathetic nerve activity evaluated by [123I]m-iodobenzylguanidine imaging in patients with ST-segment elevation myocardial infarction. *Heart*. 2011;97(1):20–26.
10. Brum PC, Rolim NP, Bacurau AV, Medeiros A. Neurohumoral activation in heart failure: the role of adrenergic receptors. *An Acad Bras Cienc*. 2006;78(3):485–503.
11. Gourine AV, et al. Astrocytes control breathing through pH-dependent release of ATP. *Science*. 2010;329(5991):571–575.
12. Marina N, et al. Purinergic signalling in the rostral ventro-lateral medulla controls sympathetic drive and contributes to the progression of heart failure following myocardial infarction in rats. *Basic Res Cardiol*. 2013;108(1):317.
13. Angelova PR, et al. Functional oxygen sensitivity of astrocytes. *J Neurosci*. 2015;35(29):10460–10473.
14. McClain JL, et al. Ca2+ responses in enteric glia are mediated by connexin-43 hemichannels and modulate colonic transit in mice. *Gastroenterology*. 2014;146(2):497–507.e1.
15. McClain JL, Fried DE, Gulbransen BD. Agonist-evoked Ca(2+) signaling in enteric glia drives neural programs that regulate intestinal motility in mice. *Cell Mol Gastroenterol Hepatol*. 2015;1(6):631–645.
16. Agulhon C, Boyt KM, Xie AX, Friocourt F, Roth BL, McCarthy KD. Modulation of the autonomic nervous system and behaviour by acute glial cell Gq protein-coupled receptor activation in vivo. *J Physiol (Lond)*. 2013;591(22):5599–5609.
17. Armbruster BN, Li X, Pausch MH, Herlitze S, Roth BL. Evolving the lock to fit the key to create a family of G protein-coupled receptors potently activated by an inert ligand. *Proc Natl Acad Sci USA*. 2007;104(12):5163–5168.
18. Agulhon C, et al. What is the role of astrocyte calcium in neurophysiology? *Neuron*. 2008;59(6):932–946.
19. Guyenet PG, Stornetta RL, Bochorishvili G, Depuy SD, Burke PG, Abbott SB. C1 neurons: the body's EMTs. *Am J Physiol Regul Integr Comp Physiol*. 2013;305(3):R187–R204.
20. Abbott SB, Stornetta RL, Socolovsky CS, West GH, Guyenet PG. Photostimulation of channelrhodopsin-2 expressing ventrolateral medullary neurons increases sympathetic nerve activity and blood pressure in rats. *J Physiol (Lond)*. 2009;587(Pt 23):5613–5631.
21. Xie AX, Lauderdale K, Murphy T, Myers TL, Fiacco TA. Inducing plasticity of astrocytic receptors by manipulation of neuronal firing rates. *J Vis Exp*. 2014;85(85):51458.
22. Nimmerjahn A, Kirchhoff F, Kerr JN, Helmchen F. Sulforhodamine 101 as a specific marker of astroglia in the neocortex in vivo. *Nat Methods*. 2004;1(1):31–37.
23. Shi H, et al. Nestin expression defines both glial and neuronal progenitors in postnatal sympathetic ganglia. *J Comp Neurol*. 2008;508(6):867–878.
24. Berthonneche C, et al. Cardiovascular response to beta-adrenergic blockade or activation in 23 inbred mouse strains. *PLoS One*. 2009;4(8):e6610.
25. Stoschitzky K, Egginger G, Zernig G, Klein W, Lindner W. Stereoselective features of (R)- and (S)-atenolol: clinical pharmacological, pharmacokinetic, and radioligand binding studies. *Chirality*. 1993;5(1):15–19.
26. Kapa S, DeSimone CV, Asirvatham SJ. Innervation of the heart: An invisible grid within a black box. *Trends Cardiovasc Med*. 2016;26(3):245–257.
27. Ferrari AU, Daffonchio A, Franzelli C, Mancia G. Potentiation of the baroreceptor-heart rate reflex by sympathectomy in conscious rats. *Hypertension*. 1991;18(2):230–235.
28. Kostrzewa RM, Jacobowitz DM. Pharmacological actions of 6-hydroxydopamine. *Pharmacol Rev*. 1974;26(3):199–288.
29. Marano G, Ramirez A, Mori I, Ferrari AU. Sympathectomy inhibits the vasoactive effects of nicotine in conscious rats. *Cardiovasc Res*. 1999;42(1):201–205.
30. Betz AJ, McLaughlin PJ, Burgos M, Weber SM, Salamone JD. The muscarinic receptor antagonist tropicamide suppresses tremulous jaw movements in a rodent model of parkinsonian tremor: possible role of M4 receptors. *Psychopharmacology (Berl)*. 2007;194(3):347–359.
31. Bonder DE, McCarthy KD. Astrocytic Gq-GPCR-linked IP3R-dependent Ca2+ signaling does not mediate neurovascular coupling in mouse visual cortex in vivo. *J Neurosci*. 2014;34(39):13139–13150.
32. Abdel-Rahman AR. Inadequate blockade by hexamethonium of the baroreceptor heart rate response in anesthetized and conscious rats. *Arch Int Pharmacodyn Ther*. 1989;297:68–85.
33. Gray SJ, et al. Optimizing promoters for recombinant adeno-associated virus-mediated gene expression in the peripheral and central nervous system using self-complementary vectors. *Hum Gene Ther*. 2011;22(9):1143–1153.
34. Zhu H, et al. Cre-dependent DREADD (designer receptors exclusively activated by designer drugs) mice. *Genesis*. 2016;54(8):439–446.
35. Feltri ML, et al. A novel P0 glycoprotein transgene activates expression of lacZ in myelin-forming Schwann cells. *Eur J Neurosci*. 1999;11(5):1577–1586.
36. Zhou P, et al. Interrogating translational efficiency and lineage-specific transcriptomes using ribosome affinity purification. *Proc Natl Acad Sci USA*. 2013;110(38):15395–15400.
37. Halassa MM, Fellin T, Haydon PG. The tripartite synapse: roles for gliotransmission in health and disease. *Trends Mol Med*. 2007;13(2):54–63.
38. Pascual O, et al. Astrocytic purinergic signaling coordinates synaptic networks. *Science*. 2005;310(5745):113–116.
39. Theis M, et al. Accelerated hippocampal spreading depression and enhanced locomotory activity in mice with astrocyte-directed inactivation of connexin43. *J Neurosci*. 2003;23(3):766–776.
40. Teubner B, et al. Connexin30 (Gjb6)-deficiency causes severe hearing impairment and lack of endocochlear potential. *Hum Mol Genet*. 2003;12(1):13–21.
41. Lalo U, Palygin O, Rasooli-Nejad S, Andrew J, Haydon PG, Pankratov Y. Exocytosis of ATP from astrocytes modulates phasic and tonic inhibition in the neocortex. *PLoS Biol*. 2014;12(1):e1001747.

42. Hanani M, Huang TY, Cherkas PS, Ledda M, Pannese E. Glial cell plasticity in sensory ganglia induced by nerve damage. *Neuroscience*. 2002;114(2):279–283.
43. Dina OA, Hucho T, Yeh J, Malik-Hall M, Reichling DB, Levine JD. Primary afferent second messenger cascades interact with specific integrin subunits in producing inflammatory hyperalgesia. *Pain*. 2005;115(1-2):191–203.
44. Hanani M. Satellite glial cells in sympathetic and parasympathetic ganglia: in search of function. *Brain Res Rev*. 2010;64(2):304–327.
45. Hanani M. Satellite glial cells in sensory ganglia: from form to function. *Brain Res Brain Res Rev*. 2005;48(3):457–476.
46. Calvert JA, Atterbury-Thomas AE, Leon C, Forsythe ID, Gachet C, Evans RJ. Evidence for P2Y1, P2Y2, P2Y6 and atypical UTP-sensitive receptors coupled to rises in intracellular calcium in mouse cultured superior cervical ganglion neurons and glia. *Br J Pharmacol*. 2004;143(5):525–532.
47. Kumagai M, Saino T. Effects of ATP on intracellular calcium dynamics of neurons and satellite cells in rat superior cervical ganglia. *Histochem Cell Biol*. 2001;115(4):285–292.
48. Gola M, Niel JP, Delmas P, Jacquet G. Satellite glial cells in situ within mammalian prevertebral ganglia express K+ channels active at rest potential. *J Membr Biol*. 1993;136(1):75–84.
49. Konishi T. Developmental and activity-dependent changes in K+ currents in satellite glial cells in mouse superior cervical ganglion. *Brain Res*. 1996;708(1–2):7–15.
50. Young JA, Brown DA, Kelly JS, Schon F. Autoradiographic localization of sites of (3H)gamma-aminobutyric acid accumulation in peripheral autonomic ganglia. *Brain Res*. 1973;63:479–486.
51. Bowery NG, Brown DA, Marsh S. gamma-Aminobutyric acid efflux from sympathetic glial cells: effect of 'depolarizing' agents. *J Physiol (Lond)*. 1979;293:75–101.
52. Wess J, Nakajima K, Jain S. Novel designer receptors to probe GPCR signaling and physiology. *Trends Pharmacol Sci*. 2013;34(7):385–392.
53. Stachniak TJ, Ghosh A, Sternson SM. Chemogenetic synaptic silencing of neural circuits localizes a hypothalamus→midbrain pathway for feeding behavior. *Neuron*. 2014;82(4):797–808.
54. Brancaccio M, Maywood ES, Chesham JE, Loudon AS, Hastings MH. A Gq-Ca2+ axis controls circuit-level encoding of circadian time in the suprachiasmatic nucleus. *Neuron*. 2013;78(4):714–728.
55. Jain S, Ruiz de Azua I, Lu H, White MF, Guettier JM, Wess J. Chronic activation of a designer G(q)-coupled receptor improves β cell function. *J Clin Invest*. 2013;123(4):1750–1762.
56. McClain JL, et al. Ca2+ responses in enteric glia are mediated by connexin-43 hemichannels and modulate colonic transit in mice. *Gastroenterology*. 2014;146(2):497–507.e1.
57. Gu Y, Chen Y, Zhang X, Li GW, Wang C, Huang LY. Neuronal soma-satellite glial cell interactions in sensory ganglia and the participation of purinergic receptors. *Neuron Glia Biol*. 2010;6(1):53–62.
58. Dunn PM, Zhong Y, Burnstock G. P2X receptors in peripheral neurons. *Prog Neurobiol*. 2001;65(2):107–134.
59. Dunn PM, Gever J, Ruan HZ, Burnstock G. Developmental changes in heteromeric P2X(2/3) receptor expression in rat sympathetic ganglion neurons. *Dev Dyn*. 2005;234(3):505–511.
60. Orellana JA, et al. ATP and glutamate released via astroglial connexin 43 hemichannels mediate neuronal death through activation of pannexin 1 hemichannels. *J Neurochem*. 2011;118(5):826–840.
61. Connolly GP, Duley JA. Ecto-nucleotidase of cultured rat superior cervical ganglia: dipyridamole is a novel inhibitor. *Eur J Pharmacol*. 2000;397(2–3):271–277.
62. Vizi ES, Liang SD, Sperlágh B, Kittel A, Jurányi Z. Studies on the release and extracellular metabolism of endogenous ATP in rat superior cervical ganglion: support for neurotransmitter role of ATP. *Neuroscience*. 1997;79(3):893–903.
63. Nacimiento W, Kreutzberg GW. Cytochemistry of 5'-nucleotidase in the superior cervical ganglion of the rat: effects of pre- and postganglionic axotomy. *Exp Neurol*. 1990;109(3):362–373.
64. Nacimiento W, Schoen SW, Nacimiento AC, Kreutzberg GW. Cytochemistry of 5'-nucleotidase in the superior cervical ganglion of cat and guinea pig. *Brain Res*. 1991;567(2):283–289.
65. Boehm S. ATP stimulates sympathetic transmitter release via presynaptic P2X purinoceptors. *J Neurosci*. 1999;19(2):737–746.
66. Boehm S. P2Ys go neuronal: modulation of Ca2+ and K+ channels by recombinant receptors. *Br J Pharmacol*. 2003;138(1):1–3.
67. Hines DJ, Haydon PG. Astrocytic adenosine: from synapses to psychiatric disorders. *Philos Trans R Soc Lond, B, Biol Sci*. 2014;369(1654):20130594.
68. Ota Y, Zanetti AT, Hallock RM. The role of astrocytes in the regulation of synaptic plasticity and memory formation. *Neural Plast*. 2013;2013:185463.
69. Giménez-Llort L, et al. Mice lacking the adenosine A1 receptor are anxious and aggressive, but are normal learners with reduced muscle strength and survival rate. *Eur J Neurosci*. 2002;16(3):547–550.
70. Ledent C, et al. Aggressiveness, hypoalgesia and high blood pressure in mice lacking the adenosine A2a receptor. *Nature*. 1997;388(6643):674–678.
71. Devaraju P, Sun MY, Myers TL, Lauderdale K, Fiacco TA. Astrocytic group I mGluR-dependent potentiation of astrocytic glutamate and potassium uptake. *J Neurophysiol*. 2013;109(9):2404–2414.
72. Hibino H, et al. Expression of an inwardly rectifying K(+) channel, Kir4.1, in satellite cells of rat cochlear ganglia. *Am J Physiol*. 1999;277(4 Pt 1):C638–C644.
73. Vit JP, Jasmin L, Bhargava A, Ohara PT. Satellite glial cells in the trigeminal ganglion as a determinant of orofacial neuropathic pain. *Neuron Glia Biol*. 2006;2(4):247–257.
74. Carozzi VA, et al. Expression and distribution of 'high affinity' glutamate transporters GLT1, GLAST, EAAC1 and of GCPII in the rat peripheral nervous system. *J Anat*. 2008;213(5):539–546.
75. Berger UV, Hediger MA. Distribution of the glutamate transporters GLAST and GLT-1 in rat circumventricular organs, meninges, and dorsal root ganglia. *J Comp Neurol*. 2000;421(3):385–399.
76. Bowery NG, Brown DA, White RD, Yamini G. [3H]gamma-Aminobutyric acid uptake into neuroglial cells of rat superior cervical sympathetic ganglia. *J Physiol (Lond)*. 1979;293:51–74.
77. Brown DA, Galvan M. Influence of neuroglial transport on the action of gamma-aminobutyric acid on mammalian ganglion

cells. *Br J Pharmacol*. 1977;59(2):373–378.
78. Shigetomi E, Tong X, Kwan KY, Corey DP, Khakh BS. TRPA1 channels regulate astrocyte resting calcium and inhibitory synapse efficacy through GAT-3. *Nat Neurosci*. 2011;15(1):70–80.
79. Liu FY, et al. Activation of satellite glial cells in lumbar dorsal root ganglia contributes to neuropathic pain after spinal nerve ligation. *Brain Res*. 2012;1427:65–77.
80. Takeda M, Takahashi M, Matsumoto S. Contribution of the activation of satellite glia in sensory ganglia to pathological pain. *Neurosci Biobehav Rev*. 2009;33(6):784–792.
81. Gu Y, Chen Y, Zhang X, Li GW, Wang C, Huang LY. Neuronal soma-satellite glial cell interactions in sensory ganglia and the participation of purinergic receptors. *Neuron Glia Biol*. 2010;6(1):53–62.
82. Gosselin RD, Suter MR, Ji RR, Decosterd I. Glial cells and chronic pain. *Neuroscientist*. 2010;16(5):519–531.
83. Hanani M. Intercellular communication in sensory ganglia by purinergic receptors and gap junctions: implications for chronic pain. *Brain Res*. 2012;1487:183–191.
84. Kanbar R, Stornetta RL, Guyenet PG. Sciatic nerve stimulation activates the retrotrapezoid nucleus in anesthetized rats. *J Neurophysiol*. 2016;116(5):2081–2092.
85. Kawabe T, Kawabe K, Sapru HN. Cardiovascular responses to somatosensory stimulation and their modulation by baroreflex mechanisms. *Clin Exp Hypertens*. 2007;29(6):403–418.
86. Pardal R, Ortega-Sáenz P, Durán R, López-Barneo J. Glia-like stem cells sustain physiologic neurogenesis in the adult mammalian carotid body. *Cell*. 2007;131(2):364–377.
87. López-Barneo J, Pardal R, Ortega-Sáenz P, Durán R, Villadiego J, Toledo-Aral JJ. The neurogenic niche in the carotid body and its applicability to antiparkinsonian cell therapy. *J Neural Transm (Vienna)*. 2009;116(8):975–982.
88. Murali S, Nurse CA. Purinergic signalling mediates bidirectional crosstalk between chemoreceptor type I and glial-like type II cells of the rat carotid body. *J Physiol (Lond)*. 2016;594(2):391–406.
89. Prabhakar NR, Semenza GL. Gaseous messengers in oxygen sensing. *J Mol Med*. 2012;90(3):265–272.
90. Feltri ML, D'Antonio M, Previtali S, Fasolini M, Messing A, Wrabetz L. P0-Cre transgenic mice for inactivation of adhesion molecules in Schwann cells. *Ann N Y Acad Sci*. 1999;883:116–123.
91. Sano Y, et al. Effects of various types of anesthesia on hemodynamics, cardiac function, and glucose and lipid metabolism in rats. *Am J Physiol Heart Circ Physiol*. 2016;311(6):H1360–H1366.
92. Schmidt RE, Chae HY, Parvin CA, Roth KA. Neuroaxonal dystrophy in aging human sympathetic ganglia. *Am J Pathol*. 1990;136(6):1327–1338.
93. Ariano MA, Briggs CA, McAfee DA. Cellular localization of cyclic nucleotide changes in rat superior cervical ganglion. *Cell Mol Neurobiol*. 1982;2(2):143–155.
94. Ariano MA, Kenny SL. Neurochemical differences in the superior cervical ganglion of the spontaneously hypertensive rat stroke-prone variant. *Brain Res*. 1987;415(1):115–121.
95. Hart EC, Charkoudian N. Sympathetic neural regulation of blood pressure: influences of sex and aging. *Physiology (Bethesda)*. 2014;29(1):8–15.
96. Adams KF, et al. Relation between gender, etiology and survival in patients with symptomatic heart failure. *J Am Coll Cardiol*. 1996;28(7):1781–1788.
97. Pothineni NV, Shirazi LF, Mehta JL. Gender differences in autonomic control of the cardiovascular system. *Curr Pharm Des*. 2016;22(25):3829–3834.
98. Hay M. Sex, the brain and hypertension: brain oestrogen receptors and high blood pressure risk factors. *Clin Sci*. 2016;130(1):9–18.
99. Vit JP, Ohara PT, Bhargava A, Kelley K, Jasmin L. Silencing the Kir4.1 potassium channel subunit in satellite glial cells of the rat trigeminal ganglion results in pain-like behavior in the absence of nerve injury. *J Neurosci*. 2008;28(16):4161–4171.
100. Vit JP, et al. Adenovector GAD65 gene delivery into the rat trigeminal ganglion produces orofacial analgesia. *Mol Pain*. 2009;5:42.
101. Ohara PT, Vit JP, Bhargava A, Jasmin L. Evidence for a role of connexin 43 in trigeminal pain using RNA interference in vivo. *J Neurophysiol*. 2008;100(6):3064–3073.
102. Narouze S. Ultrasound-guided stellate ganglion block: safety and efficacy. *Curr Pain Headache Rep*. 2014;18(6):424.
103. Guirguis M, Abdelmalak J, Jusino E, Hansen MR, Girgis GE. Stellate ganglion block for the treatment of hot flashes in patients with breast cancer: a literature review. *Ochsner J*. 2015;15(2):162–169.
104. Lipov E, Kelzenberg B. Sympathetic system modulation to treat post-traumatic stress disorder (PTSD): a review of clinical evidence and neurobiology. *J Affect Disord*. 2012;142(1-3):1–5.
105. Tian L, et al. Imaging neural activity in worms, flies and mice with improved GCaMP calcium indicators. *Nat Methods*. 2009;6(12):875–881.
106. Regan MR, et al. Variations in promoter activity reveal a differential expression and physiology of glutamate transporters by glia in the developing and mature CNS. *J Neurosci*. 2007;27(25):6607–6619.
107. Fiacco TA, et al. Selective stimulation of astrocyte calcium in situ does not affect neuronal excitatory synaptic activity. *Neuron*. 2007;54(4):611–626.
108. Guettier JM, et al. A chemical-genetic approach to study G protein regulation of beta cell function in vivo. *Proc Natl Acad Sci USA*. 2009;106(45):19197–19202.
109. van den Buuse M, Morris M, Chavez C, Martin S, Wang J. Effect of adrenalectomy and corticosterone replacement on prepulse inhibition and locomotor activity in mice. *Br J Pharmacol*. 2004;142(3):543–550.
110. Mussche S, et al. Restoration of cytoskeleton homeostasis after gigaxonin gene transfer for giant axonal neuropathy. *Hum Gene Ther*. 2013;24(2):209–219.
111. Lukashchuk V, Lewis KE, Coldicott I, Grierson AJ, Azzouz M. AAV9-mediated central nervous system-targeted gene delivery via cisterna magna route in mice. *Mol Ther Methods Clin Dev*. 2016;3:15055.